THE ASTROPHYSICAL JOURNAL, 514:249–271, 1999 March 20

LONG-TERM SCINTILLATION STUDIES OF PULSARS. II. REFRACTIVE EFFECTS AND THE SPECTRUM OF PLASMA DENSITY FLUCTUATIONS

N. D. RAMESH BHAT, YASHWANT GUPTA, AND A. PRAMESH RAO
National Centre for Radio Astrophysics, Tata Institute of Fundamental Research, Post Bag 3, Ganeshkhind, Pune-411 007, India
Received 1998 April 20; accepted 1998 October 26

ABSTRACT

Refractive scintillation effects in pulsars are powerful techniques for discriminating between different models proposed for the electron density fluctuation spectrum in the interstellar medium. Data from our long-term scintillation study of 18 pulsars in the dispersion measure range 3–35 pc cm^{-3} (Paper I) are used to investigate two important observable effects of refractive scintillation, viz., (1) modulations of diffractive scintillation observables and flux density, and (2) drifting bands in dynamic scintillation spectra. Our data provide simultaneous measurements of decorrelation bandwidth, scintillation timescale, flux density, and drift rate of patterns. The observed modulations of the first three are compared with the available theoretical predictions, and constraints are placed on the power spectrum of plasma density fluctuations. The measured modulation indices are found to be larger than predicted by a Kolmogorov form of density spectrum. The properties of the drift rate of patterns along with the diffractive scintillation parameters have been used to estimate independently the slope of the density power spectrum, which is found to be consistent with a Kolmogorov form for several pulsars. The contradictory results from these two independent methods of constraining the electron density spectrum are not reconcilable with the simple theoretical models based on power-law forms of density spectrum. Our observations show anomalous scintillation behavior such as persistent drifting bands for some pulsars. This can be interpreted as an excess power in the low wavenumber range ($\sim 10^{-12}$ to 10^{-13} m^{-1}) compared to the Kolmogorov expectations, or the existence of localized density structures. The results from our observations are discussed in combination with those from earlier studies in an attempt to understand the overall nature of the density spectrum. The emerging picture is a Kolmogorov-like spectrum ($\alpha \approx 11/3$) in the wavenumber range $\sim 10^{-6}$ m^{-1} to $\sim 10^{-11}$ m^{-1}, which either steepens or has a bump near $\sim 10^{-12}$ to 10^{-13} m^{-1}. The accumulated data also suggest the existence of discrete density structures along some lines of sight. We also discuss the possible implications of our results for the theoretical models.

Subject headings: ISM: general — ISM: structure — pulsars: general — scattering — turbulence

1. INTRODUCTION

The recognition of interstellar propagation effects in the long-term flux variations of pulsars (Sieber 1982) led to the discovery of a new class of propagation effects in radio astronomy, known as refractive interstellar scintillation (RISS) (Rickett, Coles, & Bourgois 1984). RISS is thought to arise from propagation through electron density inhomogeneities of spatial scales much larger than the Fresnel scale. In contrast to diffractive interstellar scintillation (DISS), applications of RISS extend beyond the field of pulsars, and it is thought to be the cause of low-frequency variability (LFV) of compact extragalactic radio sources. Theoretical treatments of the observable consequences of refractive scintillation can be found in Cordes, Pidwerbetsky, & Lovelace (1986) and Romani, Narayan, & Blandford (1986) (for recent reviews see also Rickett 1990; Narayan 1992; Hewish 1992). Pulsars are excellent objects for studying both DISS and RISS. In addition to the familiar long-term (days to weeks at meter wavelengths) flux variations, refractive scintillation effects are expected to give rise to slow modulations (timescales of the order of days to weeks) of DISS observables such as decorrelation bandwidth (v_d) and scintillation timescale (τ_d). Refraction due to large-scale density irregularities also gives rise to organized features such as sloping patterns in pulsar dynamic spectra (e.g., Smith & Wright 1985; Roberts & Ables 1982). RISS can also give rise to not so easily observable effects, such as variations in the pulse arrival times and angular wandering of the apparent source positions. While DISS effects probe the density irregularities of spatial scales $\sim 10^6$–10^8 m, RISS effects enable us to probe irregularities of much larger spatial scales ($\sim 10^{10}$–10^{12} m). Therefore, simultaneous measurements of DISS and RISS properties are a powerful method of determining the nature of the electron density spectrum over a much wider range than that which has been possible using DISS alone.

The density fluctuations can be characterized by their spatial wavenumber spectrum, for which there are various potential forms. The spectrum can be taken as an "extended power law" with the following general form (e.g., Rickett 1990):

$$P_{\delta n_e}(\kappa) = C_n^2(\kappa^2 + \kappa_{\rm out}^2)^{-\alpha/2} \exp\left(-\frac{\kappa^2}{\kappa_{\rm inn}^2}\right), \qquad (1)$$

where κ is the spatial wavenumber, inversely related to the length scale s (we use the relation $\kappa = 1/s$, in accordance with the convention of Armstrong, Rickett, & Spangler 1995), $\kappa_{\rm inn}$ and $\kappa_{\rm out}$ correspond to the inner and outer cutoffs in scale sizes, respectively. The amplitude of the spectrum, C_n^2, is also known as the strength of turbulence. The line-of-sight integral of equation (1) is a measure of the rms of electron density fluctuations, δn_e. The spectrum can be represented by a simpler form, $P_{\delta n_e}(\kappa) = C_n^2\,\kappa^{-\alpha}$ in the range $\kappa_{\rm out} \ll \kappa \ll \kappa_{\rm inn}$. The possibility that is most commonly discussed in the literature is the density fluctuations describable by a Kolmogorov spectrum, in which case $\alpha = 11/3$.

We refer to this as hypothesis I. Two possible subsets of this hypothesis that may be relevant are (IA) the cutoffs are not important (i.e., an inner scale much smaller than the smallest scale that influences the scintillation and an outer scale much larger than the largest scale sampled by the observations), and (IB) the spectrum is truncated at a large inner scale (say, intermediate between diffractive and refractive scales). The second possibility is that the spectrum is a simple power law (similar to hypothesis IA), but with $\alpha > 11/3$. We will call this hypothesis II. The third possibility is that the density fluctuations are *not* describable by a simple power-law form over the entire range of spatial scales of interest: this can lead to a multicomponent, "piecewise power-law" form (hypothesis IIIA) or a single power law with an additional "bump" (hypothesis IIIB) at wavenumbers corresponding to density structures that are not part of the power-law process. The fourth possibility is that the random medium (say, described by one of the above-stated hypotheses) has deterministic structures superposed, in which case a power spectral description may not be adequate. We will call this hypothesis IV. The exact form of the spectrum, especially the validity of a simple power-law description and the existence of inner and/or outer cutoff(s), is still a matter of research. In this paper our main goal is to discriminate between the above hypotheses using the data from our long-term pulsar observations.

Observable effects of RISS are considered to be powerful techniques for discriminating between different kinds of density spectra proposed for the ISM (e.g., Hewish, Wolszczan, & Graham 1985; Rickett 1990). Refractive modulation characteristics such as depths of modulations of DISS observables (v_d and τ_d), flux, and drift slope are all thought to be highly sensitive to the spectral form (e.g., Romani et al. 1986). But not all possible models indicated by hypotheses I–IV have been analyzed in detail. The *pure* Kolmogorov form (type IA) is the best analyzed of all, and there are well-defined predictions for the magnitudes of observable effects. The type II spectra have also been analyzed to some extent (e.g., Blandford & Narayan 1985; Romani et al. 1986). Three specific cases for which detailed analysis can be found in the literature are (1) $\alpha = 11/3$, (2) $\alpha = 4$ ("critical" spectrum), and (3) $\alpha = 4.3$. The effects analyzed include depths of modulations and timescales of fluctuations for different observables, refractive angle perturbations, scaling laws, and cross-correlation properties between the fluctuations. While models based on hypothesis IA predict small-amplitude fluctuations of DISS observables and flux, and small refractive perturbations ($\theta_{\rm ref} < \theta_{\rm diff}$), those based on hypothesis II can allow much larger fluctuations and large refractive angles ($\theta_{\rm ref} \gtrsim \theta_{\rm diff}$) (Romani et al. 1986; Hewish et al. 1985). It has also been recognized that a type IB spectrum, which has been suggested as an alternative to a type II spectrum, can cause large-amplitude flux modulations (Coles et al. 1987; Goodman et al. 1987). Effects (particularly perturbations on DISS observables) due to spectra grouped under hypothesis III have not been formally analyzed. Observations such as periodicities seen in pulsar dynamic spectra and "extreme scattering events" (ESE) seen toward some quasars and the millisecond pulsar PSR B1937+21 suggest that models based on hypothesis IV are also relevant (e.g., Cordes & Wolszczan 1986; Fiedler et al. 1987; Cognard et al. 1993).

Observationally, there are a number of ways of investigating the nature of the density fluctuation spectrum. But there have been conflicting interpretations from different measurements. The results from methods such as frequency scaling of decorrelation bandwidths (Cordes, Weisberg, & Boriakoff 1985), frequency drifts in dynamic spectra (e.g., Smith & Wright 1985), and VLBI observations (Gwinn et al. 1988a; Gwinn, Moran, & Reid 1988b), are consistent with the Kolmogorov spectrum. On the other hand, based on a study of dispersion measure (DM) variability, Phillips & Wolszczan (1991) find the spectrum to be much steeper ($\langle\alpha\rangle \approx 3.84 \pm 0.02$). Backer et al. (1993) studied pulsars with comparatively larger DMs, and argue that DM variations are caused by density fluctuations unrelated to those responsible for DISS. Contradictory results have come from flux monitoring observations of pulsars (Kaspi & Stinebring 1992; Gupta, Rickett, & Coles 1993; LaBrecque et al. 1994). Observations of dynamic spectra at 408 MHz (for six pulsars) by Gupta, Rickett, & Lyne (1994) show the modulations of decorrelation bandwidths to be larger than the Kolmogorov expectations, but Cordes et al. (1990) find the modulations of PSR B1937+21 to be consistent with the Kolmogorov predictions. Further, observations of quasi-periodic patterns in dynamic spectra (e.g., Cordes & Wolszczan 1986) and detections of ESEs toward some quasars (Fiedler et al. 1987, 1994) go against the Kolmogorov expectations.

Attempts have also been made to construct a *composite* spectrum by combining a variety of scintillation measurements from different observations and for various pulsars and radio sources. The most recent study by Armstrong et al. (1995) finds the *average* spectral index to be ≈ 3.7 over the wavenumber range 10^{-13} to 10^{-8} m^{-1} for pulsars within 1 kpc. They also find that, when combined with non-ISS measurements, the spectrum has an *approximately* power-law form between 10^{-18} and 10^{-6} m^{-1}. Although this result is interesting, there is enough evidence in the literature suggesting that the distribution of scattering material within a region of 1 kpc around the Sun is not homogeneous (Bhat, Gupta, & Rao 1997, 1998a). Furthermore, evidence for inadequacies of such a model can be seen in the composite spectrum of Armstrong et al. (1995), in which the estimated power levels are discrepant from the power-law expectations at several places. It is also possible that the nature of the density spectrum varies with the direction (l, b) and the location in the Galaxy, but this aspect has not been systematically investigated so far.

Observational data from a systematic long-term study of diffractive and refractive scintillations of 18 pulsars have been presented in our previous paper (Bhat, Rao, & Gupta 1998b, hereafter Paper I). These observations have yielded fairly accurate estimates of properties of observables such as decorrelation bandwidth (v_d), scintillation timescale (τ_d), flux density (F), and drift rate of patterns (dt/dv). Although our sample consists of mostly nearby pulsars (distance $\lesssim 1$ kpc), there is a reasonably uniform coverage in (l, b), DM, and distance, and the sample formed is more or less unbiased. Furthermore, we have made simultaneous measurements of DISS and RISS properties from our data, thereby reducing the possibility of observational bias. In this paper, we investigate two important and easily observable effects that can be studied using our data, viz., (1) modulations of DISS observables and flux density and (2) drifting of intensity patterns. We examine the conformity of our data with the available quantitative predictions (for type IA and II spectra) and discuss the possible implications of our results

for the form of the density spectrum.

The remainder of this paper is organized as follows. In § 2.1 we present our measurements of modulation indices (of v_d, τ_d, and F) and compare them with the theoretical predictions based on power-law models. Then we describe the estimation of statistical properties of diffractive and refractive angles with which we estimate a slope parameter, indicative of the relative power level enhancement at large scales (§ 2.2). This is followed by a discussion on persistent drifting features seen for some pulsars (§ 2.3), which suggest the presence of discrete structures, at least along some lines of sight. In § 3 we discuss the significance of various results from our observations and several others from the published literature, and study the implications for the nature of the density spectrum. Our conclusions are presented in § 4.

2. THE OBSERVATIONAL DATA AND RESULTS

The observational data used here come from an extensive series of scintillation measurements of 18 pulsars in the DM range 3–35 pc cm^{-3} made using the Ooty Radio Telescope (ORT) at 327 MHz over a 3 year period from 1993 to 1995. Pulsars and the periods of observation are tabulated in columns (2) and (3) of Table 3. The dynamic scintillation spectra of these pulsars were obtained at $\sim$10–90 epochs spanning periods ranging from $\sim$100 days to $\sim$1000 days. Columns (4) and (5) of Table 3 give the number of epochs of observation ($N_{\rm ep}$) and the time span of observation ($T_{\rm sp}$), respectively. The observations and the analysis methods used are described in Paper I.

The observations were carried out in four well-separated sessions, each extending over a period of $\sim$100 days, in which six to eight pulsars were regularly monitored for their dynamic spectra at intervals of 1–2 days typically. Four pulsars—PSR B0823+26, PSR B0834+06, PSR B1133+16, and PSR B1919+21—were followed up for multiple observing sessions: PSR B0823+06 and PSR B1919+21 for two sessions, PSR B1133+16 for three sessions, and PSR B0834+06 for all four sessions. The symbols I–IV, when attached along with these pulsar names, indicate the data from a particular session (see Tables 1 and 2 of Paper I for more details). Most of the basic diffractive scintillation results have been presented in Paper I, including the time series of decorrelation bandwidth (v_d), scintillation timescale (τ_d), drift slope of intensity patterns (dt/dv), and pulsar flux density (F) (Figs. 4*a*–4*x* of Paper I). In the present paper we start with these time series and study their implications for the spectrum of the electron density fluctuations in the ISM.

2.1. *Refractive Modulations of Diffractive Scintillation Observables and Pulsar Flux Density*

2.1.1. *Predictions from Theoretical Models*

Due to refractive scintillation effects, measurable quantities such as v_d, τ_d, dt/dv, and F are expected to fluctuate with time. Several authors have addressed the theory of refractive effects in pulsar scintillation (e.g., Cordes et al. 1986; Romani et al. 1986), but only a few attempts have been made so far in measuring and verifying them. The observable effects of RISS are thought to be highly sensitive to the form of the density spectrum, more specifically the relative power level enhancement at large scales compared to that at small scales. Romani et al. (1986) have worked out the theory for refractive effects due to simple power-law forms of density spectra with different spectral indices (covered under hypotheses IA and II of § 1). No explicit predictions are available at present for other kinds of spectra, such as those covered under hypotheses III and IV of § 1.

Considering specific cases of $\alpha = 11/3$ (Kolmogorov spectrum), $\alpha = 4$ ("critical" spectrum), and $\alpha = 4.3$ ("steep" spectrum), Romani et al. (1986) find that the depth of modulation is the lowest for a Kolmogorov density spectrum, and increases for larger values of α. In the simplest scattering geometry of a thin screen located midway between pulsar and observer, the magnitude of fluctuations of the quantities v_d, τ_d, and F will depend on (1) the strength of scattering (C_n^2), (2) observing wavelength ($\lambda_{\rm obs}$), and (3) distance to the pulsar (D), when the distribution of density irregularities follows a Kolmogorov form of power spectrum (hypothesis IA). In contrast, the fluctuations are expected to be insensitive to these parameters for $\alpha = 4$ and $\alpha = 4.3$ spectra (hypothesis II). Using the expressions given by Romani et al. (1986), for the $\alpha = 11/3$ spectrum, the modulation indices of decorrelation bandwidth (m_b), scintillation timescale (m_t), and flux density (m_r) are given by

$$m_b \approx 9.8 \times 10^{-2} \times (C_n^2)^{-0.2} (\lambda_{{\rm obs},m})^{-0.6} (D_{\rm kpc})^{-0.4}\,, \quad (2)$$

$$m_t \approx 4.8 \times 10^{-2} \times (C_n^2)^{-0.2} (\lambda_{{\rm obs},m})^{-0.6} (D_{\rm kpc})^{-0.37}\,, \quad (3)$$

$$m_r \approx 1.2 \times 10^{-1} \times (C_n^2)^{-0.12} (\lambda_{{\rm obs},m})^{-0.57} (D_{\rm kpc})^{-0.37}\,, \quad (4)$$

where C_n^2 is expressed in units of 10^{-4} m$^{-20/3}$. Using these expressions, we obtain the predicted estimates for m_b, m_t, and m_r for the pulsars in our data set. These are given in columns (4), (5), and (6) of Table 1. For C_n^2 values, we use our results given in Paper I. For pulsars with multiple observing sessions, the average of C_n^2 estimates from different sessions is used. Distance estimates used (given in col. [3] of Table 1) are based on the model for electron density distribution given by Taylor & Cordes (1993), except for PSR B0823+26, for which we use the independent distance estimate from parallax measurements (Gwinn et al. 1986). The approximate predictions for "steeper" spectra, $\alpha = 4$ and $\alpha = 4.3$, are listed in Table 2 (see Romani et al. 1986 for details).

2.1.2. *Results: Modulation Indices of v_d, τ_d, and F*

From the time series presented in Figures 4*a*–4*x* of Paper I, we estimate the modulation indices of v_d, τ_d, and F. The rms fluctuations of any of these quantities (say v_d) is given by

$$\Delta v_d \approx \left[\frac{1}{N_{\rm ep}} \sum_{i=1}^{i=N_{\rm ep}} (v_{d,i} - \langle v_d \rangle)^2\right]^{0.5}\,, \quad (5)$$

where $N_{\rm ep}$ is the number of epochs of observations and $v_{d,i}$ denotes the measurement at the ith epoch. The modulation indices m_b, m_t, and m_r, which are the fractional rms fluctuations of v_d, τ_d, and F, respectively, are given by

$$m_b = \frac{\Delta v_d}{\langle v_d \rangle}\,, \quad m_t = \frac{\Delta \tau_d}{\langle \tau_d \rangle}\,, \quad m_r = \frac{\Delta F}{\langle F \rangle}\,, \quad (6)$$

where $\langle v_d \rangle$, $\langle \tau_d \rangle$, and $\langle F \rangle$ represent the average estimates. We use the values $v_{d,g}$ and $\tau_{d,g}$ obtained from the global autocovariance function (GACF) method described in Paper I as estimators for $\langle v_d \rangle$ and $\langle \tau_d \rangle$. The mean flux density, $\langle F \rangle$, is computed directly from the time series.

TABLE 1

PREDICTED REFRACTIVE MODULATIONS[a] FOR $\alpha = 11/3$ SPECTRUM

			PREDICTED MODULATION INDICES		
			Decorrelation Bandwidth (ν_d)	Scintillation Timescale (τ_d)	Flux Density (F)
NUMBER (1)	PULSAR (2)	D (pc) (3)	m_b (4)	m_t (5)	m_r (6)
1	PSR B0329+54	1430	0.09	0.04	0.11
2	PSR B0628−28	2140	0.10	0.05	0.12
3	PSR B0823+26	380[b]	0.11	0.05	0.13
4	PSR B0834+06	720	0.11	0.05	0.14
5	PSR B0919+06	2970[c]	0.10	0.05	0.12
6	PSR B1133+16	270	0.13	0.06	0.15
7	PSR B1237+25	560	0.13	0.06	0.16
8	PSR B1508+55	1930	0.10	0.05	0.12
9	PSR B1540−06	1160	0.09	0.04	0.11
10	PSR B1604−00	590	0.11	0.05	0.13
11	PSR B1747−46	1080	0.09	0.05	0.11
12	PSR B1919+21	660	0.12	0.06	0.14
13	PSR B1929+10	170	0.14	0.06	0.16
14	PSR B2016+28	1100	0.10	0.05	0.12
15	PSR B2020+28	1300	0.10	0.05	0.12
16	PSR B2045−16	640	0.12	0.06	0.14
17	PSR B2310+42	960	0.08	0.04	0.10
18	PSR B2327−20	490	0.10	0.05	0.12

[a] Based on the theoretical expressions given by Romani, Narayan, & Blandford 1986.
[b] Distance estimate from parallax measurements (Gwinn et al. 1986).
[c] Lower limit on the distance estimate.

Before seriously interpreting our results in terms of refractive scintillation, one needs to examine (1) the statistical reliability of the data and (2) various possible reasons (other than RISS) for the fluctuations of the quantities. In addition to the number of measurements ($N_{\rm ep}$), the number of refractive cycles spanned ($N_{\rm ref}$) also determines the statistical quality of our data. On the basis of $N_{\rm ep}$ and $N_{\rm ref}$, we have divided our data into three broad categories, the details of which are given in Appendix A and the results are summarized in columns (8) and (9) of Table 3. The statistical reliability is best for data belonging to category "A" and reasonably good for those in category "B." The data that fall in either of the "C" categories are considered to be of poor statistical quality and are not taken seriously in our comparison with the predictions.

The measured modulation indices range from 0.17 to 0.50 for ν_d, from 0.13 to 0.49 for τ_d, and from 0.21 to 0.69 for F. In general, values of m_t are comparatively smaller than those of m_b and m_r, and this is in qualitative agreement with the predictions given in Tables 1 and 2. A visual examination of the time series, Figures 4*a*–4*x* of Paper I, shows that the observed fluctuations are generally random, but there are a few exceptions where some systematic trends can be seen over the time span of observation. A closer inspection of the time series of τ_d measurements of PSR B2327−20 (Fig. 4*x* of Paper I) reveals a systematic downward trend where τ_d changes from $\sim$1000 to $\sim$200 s over a span of 65 days. This is responsible for a substantially large value of m_t (0.49 ± 0.03) for this pulsar compared to the rest. Excluding this outlier case, and also the data with poor statistical reliability, we find that m_t values range from 0.13 to 0.31. For PSR B1604−00 and PSR B2016+28, some systematic trends are evident in their flux density time series. The modulation indices are, however, not significantly higher than those of the rest. Excluding the data with poor statistical quality, we find m_r values ranging from 0.23 to 0.57. The global average modulation indices are 0.36 for ν_d, 0.19 for τ_d, and 0.45 for F.

There are various sources of errors and non-ISS effects that contribute to the observed modulation index. These include (*a*) measurement noise, $\sigma_{\rm meas}$ (applicable for all the 3 quantities), (*b*) the effect of variable Faraday rotation on flux density modulations, and (*c*) the effect of Earth's orbital motion on modulations of the scintillation timescale. A

TABLE 2

PREDICTED REFRACTIVE MODULATIONS FOR STEEPER SPECTRA[a]

	PREDICTED MODULATION INDICES		
SPECTRAL INDEX (α) (1)	Decorrelation Bandwidth m_b (2)	Scintillation Timescale m_t (3)	Flux Density m_r (4)
4	0.35	0.17	0.38
4.3	0.57	0.25	0.55

[a] From Romani, Narayan, & Blandford 1986. These are only approximate predictions (correction factor γ is taken to be unity).

TABLE 3

STATISTICAL QUALITY AND RELIABILITY OF THE DATA

NUMBER (1)	PULSAR (SESSION) (2)	PERIOD OF OBSERVATION (3)	N_{ep} (4)	T_{sp} (days) (5)	τ_{ref} (days) (6)	N_{ref} (7)	RELIABILITY	
							Cycles (8)	Measurements (9)
1.....	PSR B0329+54	1995 Apr–Jul	14	67	14.1	5	B	B
2.....	PSR B0628−28	1993 Oct–1994 Jan	17	84	17.0	5	B	B
3.....	PSR B0823+26(I)	1993 Mar–May	12	67	3.7	18	A	B
4.....	PSR B0823+26(II)	1993 Oct–1994 Jan	19	88	3.6	24	A	B
5.....	PSR B0834+06(I)	1993 Jan–May	27	121	6.0	20	A	A
6.....	PSR B0834+06(II)	1993 Oct–1994 Jan	18	75	6.6	11	A	B
7.....	PSR B0834+06(III)	1994 Feb–Jun	21	79	5.2	15	A	A
8.....	PSR B0834+06(IV)	1995 Apr–Jul	27	101	3.9	26	A	A
9.....	PSR B0919+06	1994 Mar–Jun	19	71	4.7	15	A	B
10	PSR B1133+16(I)	1993 Jan–Feb	6	20	1.3	16	A	C
11	PSR B1133+16(II)	1994 Feb–Jun	25	91	1.5	60	A	A
12	PSR B1133+16(III)	1995 Apr–Jul	27	96	1.1	86	A	A
13	PSR B1237+25	1993 Oct–1994 Jan	9	78	1.8	43	A	C
14	PSR B1508+55	1995 Apr–Jul	9	53	6.2	9	B	C
15	PSR B1540−06	1995 Apr–Jul	12	92	35.8	3	C	B
16	PSR B1604−00	1995 Apr–Jul	10	94	18.6	5	B	B
17	PSR B1747−46	1995 Apr–Jul	12	93	10.5	9	B	B
18	PSR B1919+21(I)	1993 Mar–May	15	60	9.8	6	B	B
19	PSR B1919+21(II)	1993 Oct–1994 Jan	48	88	4.4	20	A	A
20	PSR B1929+10	1994 Mar−Jun	9	43	2.0	21	A	C
21	PSR B2016+28	1993 Oct–1994 Jan	20	84	36.5	2	C	A
22	PSR B2020+28	1994 Mar–Jun	15	75	7.8	10	A	B
23	PSR B2045−16	1993 Oct–1994 Jan	35	86	1.9	44	A	A
24	PSR B2310+42	1995 Apr–Jul	10	78	20.5	4	C	B
25	PSR B2327−20	1994 Mar–Jun	18	69	12.2	6	B	B

NOTE.—Multiple entries of some pulsars indicate distinct observing sessions.

detailed treatment of these noise sources is presented in Appendix B, and the estimates of their contributions are summarized in Tables 4, 5, and 6. The modulation indices due to the measurement noise are typically 0.1, and hence their contributions to the measured modulation indices are only marginal for most of the data sets (see Table 4). The noise-corrected modulation indices of v_d, τ_d, and F are given in columns (6), (7), and (8), respectively, of Table 4. Further, as can be seen from Tables 5 and 6, the effects of variable Faraday rotation and the Earth's orbital motion are significant only for a few pulsars.

2.1.3. *Comparison with the Predictions*

Taking into consideration various sources of errors and non-ISS effects discussed in Appendix B, and eliminating the data where such effects are found to be significant, we do a comparison study between the measured and predicted values of modulation indices. Here we confine ourselves to the time series of 18 data sets where the statistical reliability is reasonable. We also exclude the τ_d modulation indices of PSR B0823+26(II) (due to $m_{\rm noise} \approx m_t$), PSR B1604−00 (due to $\delta t_{\rm vobs} \approx m_t$ and $\delta t_{\rm virr} \approx m_t$) and PSR B2327−20 (due to the presence of a systematic trend in the time series) from the present comparison. In general, we find most of the modulation indices (of v_d, τ_d, and F) to be considerably larger than the Kolmogorov predictions given in Table 1, but there are a few exceptions. The details are as follows:

1. *Flux density.*—There is no pulsar for which the measured value of m_r is in agreement with the predicted value given in Table 1. While 12 of the measurements lie within the range between the predictions for $\alpha = 4$ and $\alpha = 4.3$ spectra (Table 2), the remaining six measurements are consistent with $11/3 < \alpha < 4$.

2. *Decorrelation bandwidth.*—There is only one measurement of m_b, PSR B1919+21(I), which agrees with the prediction given in Table 1. Among the rest, 14 range between the predictions for $\alpha = 4$ and $\alpha = 4.3$ (Table 2), while three are between the predictions for $\alpha = 11/3$ and $\alpha = 4$.

3. *Scintillation timescale.*—Only two measurements of m_t, PSR B0834+06(II) and PSR B0834+06(III), agree with the predictions in Table 1. The rest of the values range between the predictions for $\alpha = 11/3$ and $\alpha = 4.3$.

Although scattering from a thin screen is taken to be a good approximation in explaining diffractive scintillation phenomena, refractive effects may differ significantly depending on the scattering geometry considered. There exist only a few theoretical treatments investigating refractive effects under more complex scattering geometries such as one or more thick screens or an extended medium. Romani et al. (1986) find that such scenarios will give rise to larger flux modulations than those caused by a thin-screen model. According to the authors, if the scattering is uniformly distributed along the line of sight, the flux fluctuations will be larger by a factor of 2.3 compared to the thin-screen model, in the case of a Kolmogorov form of spectrum (i.e., hypothesis IA of § 1). Coles et al. (1987) have also investigated the flux modulations for an extended medium, and their predicted modulation indices are comparable to those of Romani et al. (1986). Similar estimates, however, do not exist for the rest of the observables of interest. On comparing the observed flux modulation indices with the predictions, we find nine of the measure-

TABLE 4

EFFECT OF NOISE ON REFRACTIVE MODULATIONS

		Noise Modulation Indices			Corrected Modulation Indices		
Number (1)	Pulsar (Session) (2)	$m_{b,\mathrm{noise}}$ (3)	$m_{t,\mathrm{noise}}$ (4)	$m_{r,\mathrm{noise}}$ (5)	$m_{b,\mathrm{riss}}$ (6)	$m_{t,\mathrm{riss}}$ (7)	$m_{r,\mathrm{riss}}$ (8)
1	PSR B0329+54	0.11	0.12	0.11	0.39	0.12	0.20[a]
2	PSR B0628−28	0.15	0.18	0.12	0.41	0.14	0.28[a]
3	PSR B0823+26(I)	0.13	0.15	0.11	0.36	0.09	0.41
4	PSR B0823+26(II)	0.15	0.15	0.11	0.32	0.00	0.35[a]
5	PSR B0834+06(I)	0.12	0.13	0.14	0.34	0.23	0.52
6	PSR B0834+06(II)	0.12	0.14	0.12	0.34	0.06	0.34[a]
7	PSR B0834+06(III)	0.10	0.12	0.11	0.18	0.05	0.34[a]
8	PSR B0834+06(IV)	0.13	0.15	0.13	0.36	0.21	0.33[a]
9	PSR B0919+06	0.09	0.10	0.11	0.24	0.16	0.48
10	PSR B1133+16(I)	0.10	0.11	0.11	0.27	0.17	0.18
11	PSR B1133+16(II)	0.12	0.11	0.13	0.42	0.29	0.21[b]
12	PSR B1133+16(III)	0.12	0.11	0.12	0.39	0.14	0.32[a]
13	PSR B1237+25	0.15	0.15	0.15	0.30	0.27	0.67
14	PSR B1508+55	0.10	0.10	0.11	0.29	0.11	0.21
15	PSR B1540−06	0.12	0.13	0.11	0.23	0.14	0.48
16	PSR B1604−00	0.13	0.13	0.14	0.42	0.10	0.45
17	PSR B1747−46	0.11	0.12	0.11	0.37	0.11	0.21[a]
18	PSR B1919+21(I)	0.11	0.12	0.13	0.13	0.17	0.47
19	PSR B1919+21(II)	0.13	0.15	0.14	0.33	0.12	0.41
20	PSR B1929+10	0.19	0.19	0.19	0.34	0.00	0.64
21	PSR B2016+28	0.16	0.17	0.16	0.44	0.29	0.37
22	PSR B2020+28	0.10	0.11	0.11	0.19	0.10	0.56
23	PSR B2045−16	0.13	0.15	0.12	0.38	0.13	0.41
24	PSR B2310+42	0.13	0.12	0.11	0.16	0.07	0.34
25	PSR B2327−20	0.13	0.14	0.13	0.48	0.47	0.30[a]

[a] Reasonable agreement with the predictions of an extended homogeneous medium with $\alpha = 11/3$.

[b] Much less than the Kolmogorov prediction (0.35) of an extended medium.

ments to be in reasonable agreement with their predicted values. For PSR B1133+16(II) , the measured value ($m_r = 0.21$) is much below the prediction (0.35). For rest of the data (nine measurements), the observed values are substantially larger than the predictions. According to Romani et al. (1986), for a spectrum with $\alpha = 4$, the flux modulation index for an extended medium is expected to be $\sqrt{3}$ times larger than that for a thin-screen model. This would mean $m_r \approx 0.66$, much above any of the measured values. Thus, excluding one measurement, the observed flux modulations are consistent with $11/3 \leq \alpha < 4$, if one considers the scattering material to be uniformly distributed along the line of sight.

Our analysis shows that the modulations due to various sources of errors and non-ISS effects (Appendices A and B) can be completely ignored for PSR B0834+06(IV) and PSR B0919+06. These data are characterized by reasonably good statistical reliability, in terms of both number of measurements and number of refractive cycles of fluctuations (Table 3). The contributions to the modulation indices (of v_d, τ_d, and F) due to the measurement noise are only marginal for these data. Also, flux modulations due to Faraday rotation effects are negligible for PSR B0834+06(IV) ($m_{r,\mathrm{pol}} \approx 0.01$) and marginal for PSR B0919+06 ($m_{r,\mathrm{pol}} \approx 0.14$). Further, effects due to the Earth's orbital motion (δt_{vobs}) and the motion of the density irregularities (δt_{virr}) can be ignored for PSR B0919+06 and are only marginal for PSR B0834+06(IV) (a worst-case reduction of 0.02 in m_t on accounting for both the effects). In addition, the data are free from effects such as persistent drift slopes and systematic trends in the time series. The results show that the modulation indices of all the three quantities are considerably above the Kolmogorov predictions. The measurements of m_b are consistent with $11/3 < \alpha \leq 4$ and that of m_t with $\alpha \approx 4$, whereas those of m_r require $4 \leq \alpha < 4.3$, as far as the predictions of a thin-screen model are concerned. If one considers an extended medium, there is agreement between the measured and predicted values of m_r for PSR B0834+06(IV) (0.33 vs. 0.32), but for PSR B0919+06, the measured value is considerably larger than the prediction (0.46 vs. 0.28).

In summary, the measured modulation indices of v_d, τ_d, and F are found to be considerably larger than the predictions of a thin-screen model with a Kolmogorov form of density spectrum (hypothesis IA of § 1). Effects due to various sources of noise involved in the measurements are insignificant except for a few values. Further, modulations due to non-ISS effects such as variable Faraday rotation and the Earth's orbital motion can be ignored for most of the data. If we compare the flux modulation indices with the predictions of a uniform scattering medium along the line of sight, roughly half of the measurements agree with the predicted values. However, similar predictions are not available at present for the modulation indices of v_d and τ_d. Clearly, theories based on a thin-screen model and hypothesis IA are inadequate to account for the results from the present observations.

2.2. *Drifting of Intensity Patterns in Dynamic Spectra*

Another important observable effect of refractive scintillation which can be studied using our data is drifting bands in dynamic spectra. The problem was addressed first by

TABLE 5

EFFECT OF VARIABLE FARADAY ROTATION ON FLUX MODULATIONS

Number (1)	Pulsar (2)	$m_{\rm lin}$ (3)	P.A. Swing (deg) (4)	RM (rad m^{-2}) (5)	$m_{r,\rm pol}$ (6)	Corrected $m_{r,\rm riss}$ (7)
1.....	PSR B0329+54	0.11[a]	105	−63.7	0.003	0.20
2.....	PSR B0628−28	0.32[a]	145	46.2	0.019	0.28
3.....	PSR B0823+26	0.29[a]	50	5.9	0.177	0.37 (I)
						0.30 (II)
4.....	PSR B0834+06	0.03[a]	140	23.6	0.005	0.52 (I)
						0.34 (II)
						0.34 (III)
						0.33 (IV)
5.....	PSR B0919+06	0.34[a]	50	32.0	0.138	0.46
6.....	PSR B1133+16	0.23[a]	90	3.9	0.103	0.15 (I)
						0.18 (II)
						0.30 (III)
7.....	PSR B1237+25	0.56[a]	30	−0.3	0.378	0.55
8.....	PSR B1508+55	0.15[a]	160[b]	0.8	0.013	0.21
9.....	PSR B1540−06	0.25[a]	25	4.0	0.170	0.45
10	PSR B1604−00	0.14[a]	110	6.5	0.048	0.45
11	PSR B1747−46	0.26[c]	90	18.0	0.102	0.18
12	PSR B1919+21	0.29[a]	25	−16.5	0.182	0.43 (I)
						0.37 (II)
13	PSR B1929+10	0.79[a]	50	−6.1	0.486	0.42
14	PSR B2016+28	0.12[d]	120	−34.6	0.023	0.37
15	PSR B2020+28	0.40[d]	120	−74.7	0.009	0.56
16	PSR B2045−16	0.27[a]	150	−10.0	0.035	0.41
17	PSR B2310+42	0.17[a]	135	7.0	0.035	0.34
18	PSR B2327−20	0.24[a]	150	9.5	0.031	0.30

NOTE.—The ionospheric contribution to RM is assumed to be $\sim$1 rad m^{-2}. The symbols I–IV indicate the observing session.

[a] Gould 1994.

[b] Measurement at 610 MHz.

[c] Hamilton et al. 1977.

[d] Manchester & Taylor 1977.

Shishov (1973) and subsequently by Hewish (1980). The basic picture is that the diffraction by small-scale irregularities (typically 10^6–10^8 m) results in an angular spectrum of scattered rays, and its mean direction of arrival is modified by the refraction through large-scale irregularities (typically 10^{10}–10^{12} m). The bending angle, $\theta_{\rm ref}$, usually known as the "refractive scattering angle," is determined by the phase gradient due to large-scale density irregularities, and is given by

$$\theta_{\rm ref} = \left(\frac{\lambda}{2\pi}\,\nabla\phi_{\rm ref}\right) \propto \left(\frac{\partial n_e}{\partial r}\right), \tag{7}$$

where λ is the observing wavelength, r is the transverse dimension, $\phi_{\rm ref}$ is the slowly varying phase component (sometimes known as the "refractive phase"), and n_e is the electron number density. The intensity patterns at the observing plane are displaced by $X \sim Z\theta_{\rm ref}$, where Z is the distance to the phase screen. The frequency dependence of the refraction angle ($\theta_{\rm ref} \propto \nu^{-2}$) results in varying magnitudes of displacements for patterns at different frequencies. In the presence of a relative motion between the pulsar and the observer, these cause intensity peaks at different frequencies to arrive at progressively increasing delays and hence appear as sloping patterns in the dynamic spectra. On elaborating the analytical treatments given by Shishov (1973), Hewish (1980) showed that the drift slope, dv/dt, can be related to the refractive steering angle, $\theta_{\rm ref}$, through the following expression:

$$\frac{dt}{dv} = \frac{D\theta_{\rm ref}}{V_{\rm iss}\, f_{\rm obs}}, \tag{8}$$

where $V_{\rm iss}$ is the speed of scintillation patterns, $f_{\rm obs}$ is the frequency of observation, and D is the separation between the source and the observer. The above expression is for a thin-screen geometry, with the screen located midway between the source and the observer ($D = 2Z$). In characterizing the drifting features in our data, we prefer dt/dv over dv/dt. Justification for this choice and our definition of drift slope is described in Paper I.

Drifting of intensity patterns is extensively seen in our data (e.g., Figs. 1*a*–1*h* of Paper I). The property is highly pronounced for PSR B0834+06, PSR B1133+16, PSR B1919+21, and PSR B2045−16. The measured values of dt/dv (see Figs. 4*a*–4*x* of Paper I) range from $\sim$0.05 s kHz^{-1} (e.g., PSR B1133+16, PSR B1237+25) to a few s kHz^{-1} (e.g., PSR B1604−00, PSR B2327−20). Also, several pulsars show gradual and systematic variations of drift slopes, along with a number of sign reversals, during the time span of observations. The data of PSR B0823+26 and PSR B0919+06 are good examples illustrating this property. In general, drift slopes are found to vary over timescales comparable to those of v_d, τ_d, and F, but our data are not sampled regularly enough to obtain robust estimates of these timescales. The drift slope averaged over all

TABLE 6

MODULATIONS OF SCINTILLATION TIMESCALE DUE TO V_{obs} AND V_{irr}

Number (1)	Pulsar (Session) (2)	$\Delta V_{obs_\perp}$ (km s^{-1}) (3)	δt_{vobs} (4)	δt_{virr} [a] (5)
1.....	PSR B0329+54	6.3	0.03	0.05
2.....	PSR B0628−28	5.3	0.03	0.06
3.....	PSR B0823+26(I)	11.4	0.05	0.04
4.....	PSR B0823+26(II)	27.5	0.10	0.04
5.....	PSR B0834+06(I)	22.6	0.14	0.06
6.....	PSR B0834+06(II)	23.5	0.12	0.05
7.....	PSR B0834+06(III)	12.2	0.05	0.04
8.....	PSR B0834+06(IV)	21.4	0.09	0.04
9.....	PSR B0919+06	13.8	0.02	0.02
10	PSR B1133+16(I)	4.0	0.01	0.02
11	PSR B1133+16(II)	20.6	0.06	0.03
12	PSR B1133+16(III)	17.0	0.04	0.03
13	PSR B1237+25	13.1	0.04	0.03
14	PSR B1508+55	1.5	0.00	0.02
15	PSR B1540−06	18.5	0.24	0.13
16	PSR B1604−00	15.1	0.24	0.16
17	PSR B1747−46	7.3	0.03	0.05
18	PSR B1919+21(I)	2.6	0.02	0.08
19	PSR B1919+21(II)	9.4	0.05	0.05
20	PSR B1929+10	8.6	0.06	0.07
21	PSR B2016+28	7.5	0.14	0.18
22	PSR B2020+28	3.8	0.02	0.05
23	PSR B2045−16	29.2	0.05	0.02
24	PSR B2310+42	3.7	0.04	0.11
25	PSR B2327−20	17.4	0.22	0.13

[a] Assuming $V_{irr} \sim 10$ km s^{-1} (Bondi et al. 1994).

the measurements of a given data set, $\langle dt/dv \rangle$, and the rms fluctuation, $\delta(dt/dv)$, are computed for each data set, and are given in columns (3) and (4) of Table 7. For several pulsars, values of $\langle dt/dv \rangle$ are found to be quite close to zero. Some pulsars, especially those characterized by few or no slope reversals, show significantly large values of average drift slopes.

2.2.1. *Pattern Drifts and Decorrelation Bandwidth*

Refractive effects, such as those which produce drifting intensity patterns, are expected to affect the estimation of the decorrelation bandwidth (e.g., Gupta et al. 1994; Cordes et al. 1986). Usually, the decorrelation bandwidth is measured as the half-width at half-maximum along the frequency lag axis of the two-dimensional autocovariance function (ACF) of the dynamic spectrum. In the absence of refractive bending, this method correctly estimates the true decorrelation bandwidth produced by DISS, as intensity patterns at different frequencies are aligned in time. However, in the presence of significant refractive bending, this method will always underestimate the decorrelation bandwidth as the drifting patterns are no longer aligned in time. Under such conditions, a better estimate can be obtained by measuring the half-power bandwidth along the direction of the drift slope rather than along the frequency lag axis. For the case where the direction of the shift of intensity patterns is aligned with the direction of the scintillation velocity (V_{iss}), the new technique will result in complete correction of the v_d value. Clearly, the effectiveness of this technique decreases as the angle between the phase gradient and V_{iss} increases from 0° to 90°.

TABLE 7

PROPERTIES OF DRIFT RATES AND CORRECTED BANDWIDTHS

Number (1)	Pulsar (Session) (2)	$\langle dt/dv \rangle$ (s kHz^{-1}) (3)	$\delta(dt/dv)$ (s kHz^{-1}) (4)	Drift Class (5)	$\langle v_{d_c} \rangle$ (kHz) (6)	$m_{b,c}$ (7)	m_{noise} (8)	$m_{b,c(riss)}$ (9)
1.....	PSR B0329+54	−0.09±0.04	0.10±0.06	NC	219	0.28	0.11	0.26
2.....	PSR B0628−28	+0.04±0.08	0.27±0.11	I	307	0.48	0.13	0.46
3.....	PSR B0823+26(I)	+0.00±0.02	0.15±0.02	I	452	0.28	0.13	0.24
4.....	PSR B0823+26(II)	−0.06±0.02	0.08±0.03	NC	338	0.27	0.16	0.22
5.....	PSR B0834+06(I)	+0.40±0.01	0.16±0.02	II	716	0.33	0.13	0.30
6.....	PSR B0834+06(II)	+0.39±0.02	0.34±0.03	II	504	0.23	0.12	0.19
7.....	PSR B0834+06(III)	+0.29±0.01	0.18±0.02	II	488	0.25	0.11	0.23
8.....	PSR B0834+06(IV)	+0.08±0.01	0.18±0.02	I	696	0.35	0.12	0.33
9.....	PSR B0919+06	+0.01±0.02	0.14±0.02	I	305	0.21	0.10	0.19
10	PSR B1133+16(I)	+0.01±0.01	0.06±0.01	I	554	0.23	0.12	0.20
11	PSR B1133+16(II)	+0.03±0.01	0.09±0.01	I	986	0.39	0.14	0.36
12	PSR B1133+16(III)	−0.05±0.01	0.06±0.01	NC	1763	0.36	0.16	0.32
13	PSR B1237+25	+0.04±0.01	0.06±0.01	NC	1241	0.50	0.16	0.47
14	PSR B1508+55	+0.01±0.03	0.07±0.04	I	268	0.27	0.10	0.26
15	PSR B1540−06	+0.22±0.12	0.27±0.17	I	195	0.10	0.12	...[a]
16	PSR B1604−00	+0.63±0.08	0.91±0.11	I	508	0.53	0.15	0.50
17	PSR B1747−46	+0.04±0.04	0.12±0.06	I	231	0.27	0.11	0.25
18	PSR B1919+21(I)	+0.39±0.03	0.26±0.04	II	424	0.15	0.13	0.07[b]
19	PSR B1919+21(II)	+0.17±0.01	0.17±0.01	II	626	0.30	0.13	0.27
20	PSR B1929+10	+0.08±0.01	0.19±0.02	I	1444	0.36	0.20	0.30
21	PSR B2016+28	+0.30±0.14	0.79±0.20	I	284	0.32	0.16	0.28
22	PSR B2020+28	−0.10±0.03	0.21±0.05	I	272	0.22	0.09	0.20
23	PSR B2045−16	+0.06±0.01	0.09±0.01	NC	671	0.33	0.11	0.32
24	PSR B2310+42	−0.18±0.09	0.17±0.12	NC	190	0.06	0.11	...[a]
25	PSR B2327−20	−0.04±0.07	0.96±0.10	I	328	0.36	0.14	0.33

[a] Noise modulations dominate over the observed fluctuations of v_{d_c}.
[b] The observed fluctuations of v_{d_c} are comparable to the noise modulations.

Thus we define a new estimator for the decorrelation bandwidth, which we refer to as the "drift-corrected decorrelation bandwidth," v_{d_c}, which is the frequency lag corresponding to the point on the half-maximum contour of the ACF that is farthest from the time lag axis. In terms of the parameters C_1, C_2, and C_3 describing the model Gaussian (eq. [2] of Paper I) fitted to the ACF, v_{d_c} can be expressed as

$$v_{d_c} = (\ln 2)^{0.5}\left(C_1 - \frac{C_2^2}{4C_3}\right)^{-0.5}. \quad (9)$$

The time series of corrected decorrelation bandwidths obtained in this manner are shown in Figures 1*a*–1*x* of this paper. These can be compared with the "instantaneous" or "apparent" decorrelation bandwidth, v_d, shown in Figure 4 of Paper I, to obtain some idea about the reduction in decorrelation bandwidth due to refractive effects. We also compute the statistical properties of v_{d_c}, such as its average value, $\langle v_{d_c}\rangle$, and fractional rms fluctuation, $m_{b,c}$, which are given in columns (6) and (7) of Table 7. Columns (8) and (9) of Table 7 give the noise modulation indices and the noise-corrected values of $m_{b,c}$, analogous to columns (3) and (6) of Table 4.

Here we briefly summarize the general characteristics of the corrected bandwidth. For most pulsars, its average value is larger than that of the traditional decorrelation bandwidth (i.e., $\langle v_{d_c}\rangle > \langle v_d\rangle$). In addition, modulation indices of v_{d_c} are generally smaller than those of v_d (i.e., $m_{b,c} \lesssim m_b$). The only exceptions are PSR B1237+25 and PSR B1604−00, for which estimates of $m_{b,c}$ are substantially larger than those of m_b. For PSR B1604−00, this is due to a few dominating measurements in the time series (Fig. 1*o*). For PSR B1540−06 and PSR B2310+42, we see that corrected bandwidths appear to be more or less stable ($m_{b,c} \lesssim 0.1$), which could be an artifact due to the limitation of our spectrometer resolution. Excluding these four outliers, we find the global average modulation index ($\langle m_{b,c}\rangle$) to be ≈ 0.3. Measurement noise is expected to cause a modulation index of 0.1 (see col. [8] of Table 7), and hence its contribution to the measured value is only marginal. The only case where noise modulations are significant is PSR B1919+21(I), where $m_{b,c} \sim m_{\rm noise}$ and we get $m_{b,c(\rm riss)} \approx 0.06$. On comparing the estimates of $m_{b,c}$ with the theoretical predictions, we find them to be considerably larger than the Kolmogorov predictions. However, in contrast to m_b, most measurements range between the predictions of $\alpha = 11/3$ and $\alpha = 4$.

The above analysis confirms that the traditional estimator for the decorrelation bandwidth (v_d) is biased because of the presence of refractive drifts that are produced by the large-scale irregularities in the ISM. The new estimator for the decorrelation bandwidth (v_{d_c}) is less prone to bias due to such refractive effects. Thus, v_{d_c} should be a better choice for estimating effects due to purely diffractive scintillation phenomena, i.e., effects produced by the small-scale irregularities in the ISM. In the following section, where we

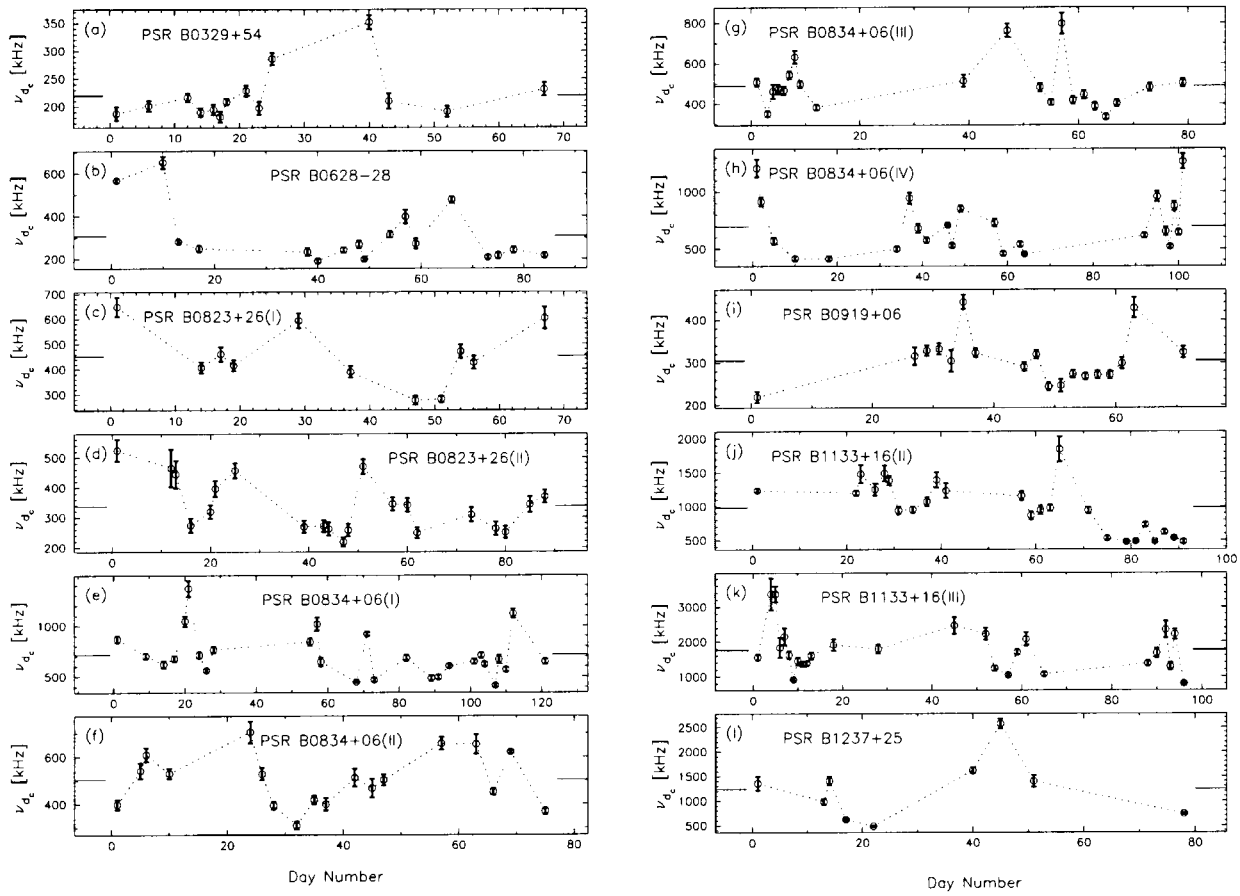

FIG. 1.—Time series of drift-corrected decorrelation bandwidth, v_{d_c}. The uncertainties in the measurements indicate $\pm 1\,\sigma$ error estimates, which include errors due to Gaussian model fitting and estimation errors due to the finite number of scintles at a given epoch of observation. The name of the pulsar and session identification (wherever needed) are given within each panel. The solid markers (at either end of the panel) indicate the average estimates of the time series.

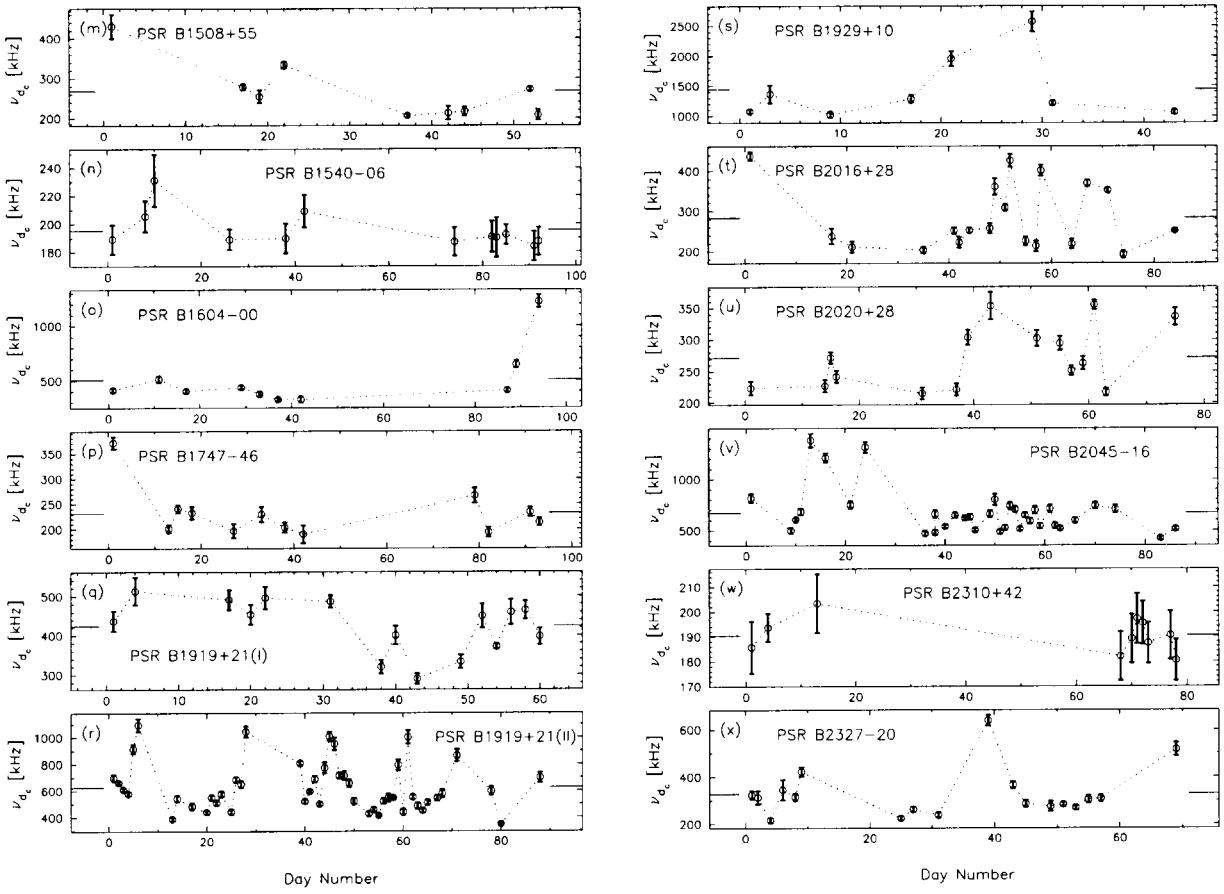

FIG. 1.—*Continued*

attempt to estimate effects of small-scale and large-scale irregularities independently, we use v_{d_c} as the estimator for the decorrelation bandwidth.

2.2.2. *Estimation of Diffractive and Refractive Scattering Angles*

Diffractive and refractive scattering angles are two useful indicators of the magnitude of electron density fluctuations at small ($\sim 10^6$–10^8 m) and large ($\sim 10^{10}$–10^{12} m) spatial scales, respectively. From our data, we estimate these two angles, denoted as $\theta_{\rm diff}$ and $\theta_{\rm ref}$, respectively, at each epoch of observation. The diffractive scattering angle at the ith epoch, $\theta_{{\rm diff},i}$, is given by

$$\theta_{{\rm diff},i} = \left(\frac{c}{\pi D \nu_{d_c,i}}\right)^{0.5}, \tag{10}$$

where $\nu_{d_c,i}$ denotes the measurement at the ith epoch of observation and c is the speed of light. We use the average diffractive angle ($\langle\theta_{\rm diff}\rangle$) over the entire time span of observation to characterize density fluctuations at small spatial scales. Our values of $\langle\theta_{\rm diff}\rangle$ are given in column (5) of Table 8.

The refractive angle at the ith epoch of observation, $\theta_{{\rm ref},i}$, is obtained from the estimates of the drift rate, $(dt/d\nu)_i$, and scintillation pattern speed, $V_{{\rm iss},i}$, at that epoch, using the relation

$$\theta_{{\rm ref},i} = \left(\frac{V_{{\rm iss},i}\, f_{\rm obs}}{D}\right)\left(\frac{dt}{d\nu}\right)_i. \tag{11}$$

We note that when the gradient of the refractive wedge is not aligned with the pattern velocity, the true refractive angle is given by $\theta_{{\rm ref},i}\sec\psi_i$, where ψ is the angle between the gradient and the velocity. For simplicity, we assume $\psi = 0$ in estimating $\theta_{{\rm ref},i}$, but address this issue later in this section. The pattern speed ($V_{\rm iss}$) is estimated from the measurements of decorrelation bandwidth and scintillation timescale, using the following expression:

$$V_{{\rm iss},i} = A_V (D_{\rm [kpc]}\, \nu_{d_c,i{\rm [MHz]}})^{0.5} (f_{\rm obs[GHz]}\, \tau_{d,i{\rm [s]}})^{-1} \text{ km s}^{-1}, \tag{12}$$

where $\tau_{d,i}$ denotes the measurement at the ith epoch of observation, and we adopt $A_V = 3.85 \times 10^4$ given by Gupta et al. (1994). Our measurements of refractive scattering angles obtained in the above manner are presented in Figures 2*a*–2*x*, in the form of the time series for each pulsar.

According to the models that treat refraction effects as random phenomena due to the low-wavenumber part of the underlying density power spectrum, $\theta_{\rm ref}$ is expected to vary randomly about a zero mean value over refractive timescales (Rickett 1990; Rickett et al. 1984; Romani et al. 1986). But treatments that consider refraction by a separate large-scale component (e.g., Shishov 1973; Hewish 1980) may allow nonzero mean values for $\theta_{\rm ref}$. The mean refractive angles ($\langle\theta_{\rm ref}\rangle$) computed from the time series in Figure 2 are listed in column (3) of Table 8. For a number of pulsars, $\langle\theta_{\rm ref}\rangle \approx 0$ within the measurement uncertainties (e.g., PSR B0919+06 and PSR B0823+26), while for some, $\langle\theta_{\rm ref}\rangle$ is found to be significantly different from zero, the best examples for which are PSR B0834+06 and PSR B1919+21. PSR B1133+16 (data from sessions II and III), PSR B1237+25, PSR B1604−00, PSR B1929+10, and PSR B2045−16 also show statistically significant nonzero values for $\langle\theta_{\rm ref}\rangle$. For PSR B1237+25 and PSR B1929+10, such

TABLE 8

ESTIMATES OF DIFFRACTIVE AND REFRACTIVE ANGLES AND SPECTRAL SLOPES

Number (1)	Pulsar (Session) (2)	$\langle\theta_{ref}\rangle$ (mas) (3)	$\delta\theta_{ref}$ [a] (mas) (4)	$\langle\theta_{diff}\rangle$ (mas) (5)	β (6)
1	PSR B0329+54	-0.02 ± 0.02	0.04 ± 0.03	0.73 ± 0.01	3.29 ± 0.21
2	PSR B0628−28	$+0.01\pm0.01$	0.07 ± 0.03	0.51 ± 0.01	3.50 ± 0.10
3	PSR B0823+26(I)	$+0.01\pm0.03$	0.34 ± 0.05	0.95 ± 0.02	3.73 ± 0.04
4	PSR B0823+26(II)	-0.10 ± 0.03	0.18 ± 0.06	1.09 ± 0.02	3.54 ± 0.09
5	PSR B0834+06(I)	$+0.24\pm0.01$	0.12 ± 0.01	0.54 ± 0.01	3.58 ± 0.03
6	PSR B0834+06(II)	$+0.25\pm0.01$	0.26 ± 0.03	0.63 ± 0.01	3.77 ± 0.03[b]
7	PSR B0834+06(III)	$+0.23\pm0.01$	0.20 ± 0.02	0.64 ± 0.01	3.69 ± 0.03
8	PSR B0834+06(IV)	$+0.07\pm0.01$	0.19 ± 0.02	0.54 ± 0.01	3.71 ± 0.03
9	PSR B0919+06	$+0.00\pm0.01$	0.10 ± 0.02	0.41 ± 0.01	3.65 ± 0.04
10	PSR B1133+16(I)	$+0.00\pm0.04$	0.33 ± 0.07	0.96 ± 0.02	3.70 ± 0.06
11	PSR B1133+16(II)	$+0.06\pm0.01$	0.36 ± 0.03	0.75 ± 0.01	3.78 ± 0.02[b]
12	PSR B1133+16(III)	-0.15 ± 0.01	0.29 ± 0.02	0.55 ± 0.01	3.80 ± 0.02[b]
13	PSR B1237+25	$+0.05\pm0.01$	0.12 ± 0.03	0.48 ± 0.01	3.51 ± 0.08
14	PSR B1508+55	-0.00 ± 0.02	0.06 ± 0.03	0.56 ± 0.01	3.44 ± 0.15
15	PSR B1540−06	$+0.03\pm0.02$	0.06 ± 0.05	0.86 ± 0.01	3.39 ± 0.18
16	PSR B1604−00	$+0.14\pm0.02$	0.33 ± 0.04	0.72 ± 0.01	3.79 ± 0.03[b]
17	PSR B1747−46	$+0.02\pm0.02$	0.08 ± 0.05	0.80 ± 0.01	3.45 ± 0.13
18	PSR B1919+21(I)	$+0.20\pm0.01$	0.20 ± 0.03	0.73 ± 0.01	3.66 ± 0.04
19	PSR B1919+21(II)	$+0.12\pm0.01$	0.16 ± 0.01	0.59 ± 0.01	3.63 ± 0.03
20	PSR B1929+10	$+0.14\pm0.03$	0.57 ± 0.05	0.76 ± 0.02	3.91 ± 0.03[b]
21	PSR B2016+28	$+0.04\pm0.02$	0.14 ± 0.03	0.72 ± 0.01	3.59 ± 0.06
22	PSR B2020+28	-0.05 ± 0.01	0.11 ± 0.03	0.66 ± 0.01	3.54 ± 0.07
23	PSR B2045−16	$+0.10\pm0.01$	0.19 ± 0.02	0.58 ± 0.01	3.69 ± 0.03
24	PSR B2310+42	-0.05 ± 0.03	0.06 ± 0.06	0.96 ± 0.02	3.38 ± 0.20
25	PSR B2327−20	-0.02 ± 0.03	0.42 ± 0.05	0.98 ± 0.01	3.78 ± 0.03[b]

[a] Measured values scaled by $\sqrt{2}$, as described in the text (§ 2.2.2).

[b] Estimates that are significantly larger than 11/3.

an effect may be attributed to the poor statistics in terms of limited number of measurements and/or dominance of a few measurements over the rest (see Figs. 2*l* and 2*s*). PSR B1133+16 and PSR B2045−16 show nonzero $\langle\theta_{ref}\rangle$ despite sufficiently good statistics ($N_{ep}=25$–35). A closer inspection of their time series of θ_{ref} (Figs. 2*j*, 2*k*, and 2*v*) reveal that, though not highly pronounced, there are some signatures of persistent drifts lasting typically over several weeks. A similar trend can also be seen for PSR B1604−00 (Fig. 2.*o*), but here the sampling is rather coarse. Thus not all our data are in support of the expectations of models based on random refraction.

As mentioned earlier, in the case of two-dimensional refraction, the observer will measure a refractive angle $\theta_{ref}=\Theta_{ref}\cos\psi$, where Θ_{ref} is the "true refractive angle" and ψ is the "alignment angle." This effect can potentially modify the statistical properties estimated for θ_{ref}. In particular, it will result in an underestimation of the rms refractive angle, $\delta\theta_{ref}$. Although an exact correction for this is not practical, we attempt a first-order correction by assuming Θ_{ref} and ψ to be independent zero-mean random variables, and also that ψ can range from $-\pi/2$ to $\pi/2$ with uniform probability. This gives $\langle\Theta_{ref}^2\rangle=2\langle\theta_{ref}^2\rangle$, which implies $\delta\Theta_{ref}=\sqrt{2}\delta\theta_{ref}$. This will yield somewhat better estimates of $\delta\theta_{ref}$, at least for data with $\langle\theta_{ref}\rangle\approx0$. The values of $\delta\theta_{ref}$ given in column (4) of Table 8 are the measured values scaled by $\sqrt{2}$.

2.2.3. *Estimation of Slope of the Electron Density Spectrum*

In this section we use the measurements of θ_{diff} and θ_{ref} to estimate the slope (α) needed for representing the underlying density fluctuations by a simple power-law form of spectrum, at least over the DISS and RISS scales of interest for our data. There are two possible ways of doing this. The first is to make use of the ratio $\delta\theta_{ref}/\langle\theta_{diff}\rangle$ as a discriminator of α. For $\alpha<4$, the refractive scattering angles are expected to be smaller than the diffractive angles ($\delta\theta_{ref}<\langle\theta_{diff}\rangle$), but for "steep" spectra ($\alpha>4$), $\delta\theta_{ref}>\langle\theta_{diff}\rangle$ can be expected (Hewish et al. 1985; Romani et al. 1986; Rickett 1990). Earlier studies (Smith & Wright 1985; Hewish et al. 1985) did not have good enough data to facilitate accurate determinations of $\delta\theta_{ref}$ and $\langle\theta_{diff}\rangle$, and often employed $\theta_{ref}/\theta_{diff}$ from a given (or a few) epoch(s) of observations to discriminate between different kinds of density spectra. For the values of $\delta\theta_{ref}$ and $\langle\theta_{diff}\rangle$ given in Table 8, we find the ratio for most of the pulsars to be in the range 0.1–0.8, and there is no pulsar for which it is above unity. Thus, if the density spectra are to be represented by simple power-law forms, then the measurements of θ_{diff} and θ_{ref} from our observations will preclude $\alpha>4$ for these epochs.

The second method is to estimate the power levels P_{ref} and P_{diff} at refractive and diffractive wavenumbers κ_{ref} and κ_{diff}, respectively, from which the slope of the density spectrum can be estimated (e.g., Armstrong et al. 1995). The procedure is as follows. From the measurements of $\delta\theta_{ref}$, one can obtain the structure function level at refractive length scale s_{ref} (given by $1/\kappa_{ref}$), from which an estimate of the amplitude of the density spectrum (C_N^2) is obtained. The power level at refractive scale is then given by $P_{ref}=C_N^2\kappa_{ref}^{-\alpha}$. From the measurements of decorrelation bandwidths, one can estimate the amplitude of the spectrum (C_n^2) at small spatial scales, and the power level at diffractive

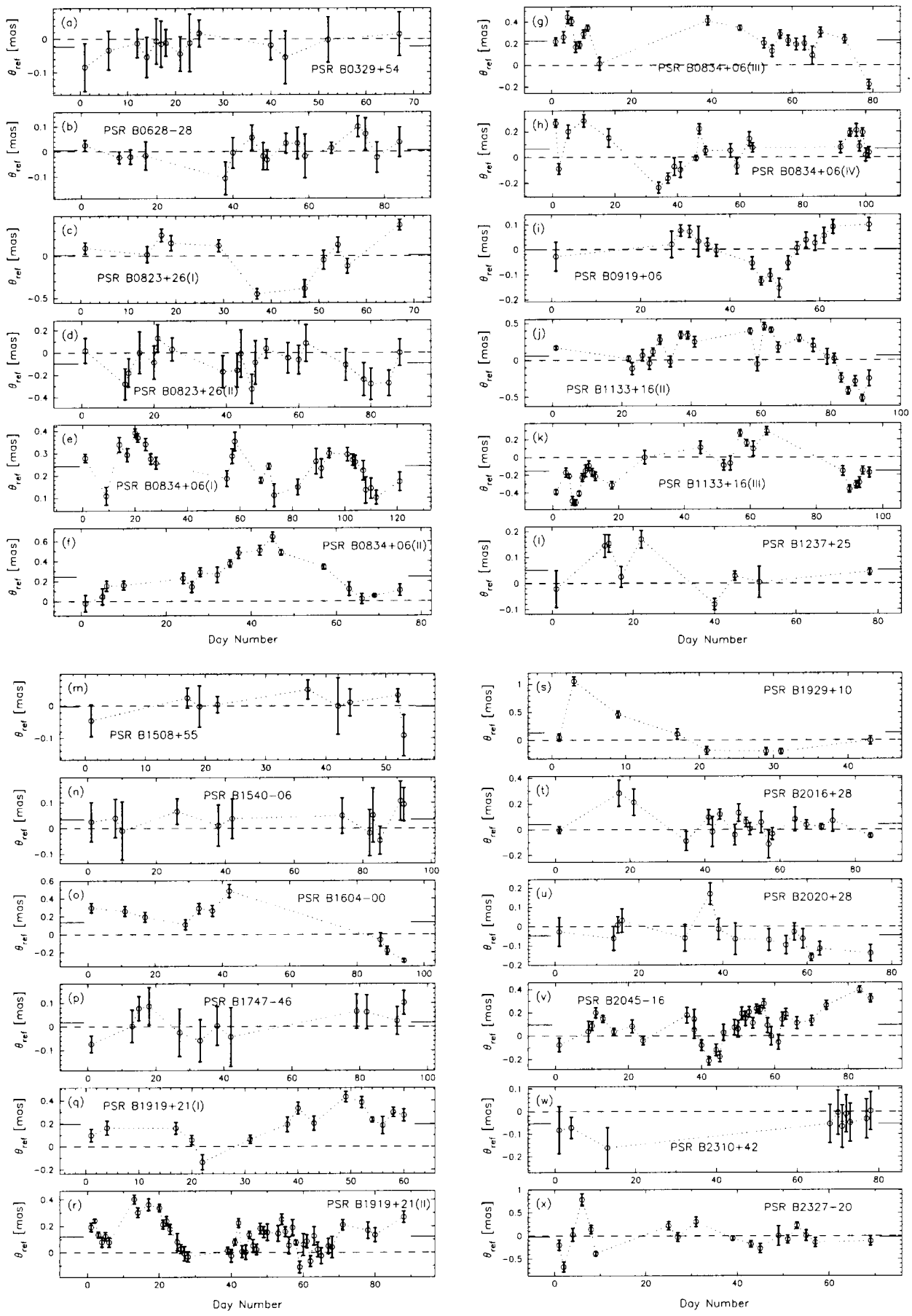

FIG. 2.—Similar to Fig. 1, except that the quantity plotted is the refractive scattering angle $\theta_{\rm ref}$. The dashed line corresponds to $\theta_{\rm ref} = 0$.

wavenumber (given by $\kappa_{\rm diff} = 1/s_0$, where s_0 is the "coherence scale") is then given by $P_{\rm diff} = C_n^2 \kappa_{\rm diff}^{-\alpha}$. This method should give $C_N^2 \approx C_n^2$ if the assumed value of α is correct. Alternatively, one can estimate a slope $\beta = \log (P_{\rm ref}/P_{\rm diff})/\log (\kappa_{\rm ref}/\kappa_{\rm diff})$. Throughout this paper, we use α to denote the power-law index (as defined in eq. [1]) of the density spectrum, and β to represent the slope estimated from our measurements.

It is easy to show that the above two methods are not independent and also that for $\alpha < 4$ there is an exact correspondence between the ratio of scattering angles ($\delta\theta_{\rm ref}/\langle\theta_{\rm diff}\rangle$) and the slope estimate, β. For this, we first rewrite equation (3) of Armstrong et al. (1995) as

$$C_n^2 = K_\alpha [D_\phi(s)](8\pi r_e^2 \lambda_{\rm obs}^2 D s^{\alpha_1})^{-1}\ , \qquad (13)$$

where $\alpha_1 = \alpha - 2$, $K_\alpha = (1 + \alpha_1)[f(\alpha_1)]^{-1}$, D is the propagation distance, and r_e is the classical electron radius. The phase structure function, D_ϕ, at refractive scale, $s_{\rm ref}$, is given by

$$D_\phi(s_{\rm ref}) \approx \left[\left(\frac{2\pi}{\lambda_{\rm obs}}\right)\delta\theta_{\rm ref}\, s_{\rm ref}\right]^2 , \qquad (14)$$

where $\lambda_{\rm obs}$ is the observing wavelength. The refractive scale can be taken as the "scattering disk," given by $\sim D\langle\theta_{\rm diff}\rangle$. The structure function is unity at coherence scale [$D_\phi(s_0) = 1$], which is also considered as the diffractive length scale, $s_{\rm diff}$. Thus, from equation (13), we can get the two estimates of the amplitude of the density spectrum, C_N^2 and C_n^2. Using these expressions, the slope estimate, β, simplifies to

$$\beta = 4 + \left[\frac{\log (\delta\theta_{\rm ref}/\langle\theta_{\rm diff}\rangle)}{\log u}\right], \qquad (15)$$

where u is a measure of the strength of scattering, defined as $(s_{\rm ref}/s_0)^{1/2}$ (Rickett 1990). The value of u can be estimated from decorrelation bandwidth measurements (see Table 4 of Paper I for our estimates). We note that equation (15) is very similar to equation (2.9) given by Rickett (1990). We also note that the above result is valid only for $\alpha < 4$, as equation (13) is valid only for this regime. From this result, one can see that, for a given value of u, the ratio of scattering angles is related to the slope of the density spectrum. Further, one can see that as $\beta \to 4$, $\delta\theta_{\rm ref} \to \langle\theta_{\rm diff}\rangle$.

Our estimates of β are given in column (6) of Table 8, and they range from 3.3 to 3.9. Since all the three quantities ($\delta\theta_{\rm ref}$, $\langle\theta_{\rm diff}\rangle$, and u) have been fairly accurately determined, we are able to estimate the values of β with fairly good accuracies (1 σ uncertainty $\sim$0.02–0.1). In some cases, the uncertainties are larger ($\sim$0.1–0.2), probably because of sloping patterns not being well pronounced in the corresponding data. Further, none of our values of β are above the critical value 4, which gives an ex post facto justification of the assumption $\alpha < 4$ made in obtaining equation (15).

Taking into consideration the uncertainties (at ± 2 σ levels), we find 18 of the 25 measurements to be consistent with the Kolmogorov value 11/3. For six data sets, the measured values are significantly above 11/3. The highest value ($\beta = 3.91 \pm 0.03$) is measured for PSR B1929+10, the closest pulsar in our sample. The other cases are PSR B1604−00 and PSR B2327−20, and part of the data of PSR B0834+06 (session II) and PSR B1133+16 (sessions II and III), with $\beta \approx 3.77$–3.8. We note that values of β that are significantly below 11/3 (i.e., $\beta \approx 3.3$–3.4) are also the ones that have large measurement errors (PSR B0329+54, PSR B1508+55, PSR B1540−06, and PSR B2310+42). Further, these are also the cases where sloping patterns are less pronounced, depending on which one tends to underestimate the dt/dv values and consequently the values of β. For one data set, PSR B0834+06(I), the estimated β ($\approx 3.58 \pm 0.03$) is significantly below the Kolmogorov index. Thus, not all the measurements from our data are consistent with a Kolmogorov form of density spectrum (hypothesis IA of § 1). The larger values of β (3.77–3.91) are seen for nearby pulsars ($\sim$200–700 pc), and there is a weak trend for a decrease in β with DM (up to $\sim$20 pc cm^{-3}) and distance (up to $\sim$1 kpc) (see Figs. 3*a* and 3*b*). Clearly, a ubiquitous nature of the density spectrum is not quite supported and there are several directions toward which the density spectrum appears to be steeper than $\alpha = 11/3$.

Before proceeding further, we comment on some of the underlying assumptions in our β estimation. First, our values of β are indicative of the true slope only if (1) the spectrum is a simple power law, and (2) $\alpha < 4$. Second, the method is subject to the validity of the implicit assumption of drifting features arising due to density fluctuations on spatial scales of the order of the scattering disk, $D\theta_{\rm diff}$. Further, the method assumes a stationary statistics for RISS, which need not necessarily be true in practice, especially for data with nonzero $\langle\theta_{\rm ref}\rangle$. Hence $\delta\theta_{\rm ref}$, and consequently β, should be treated with caution for those cases. In the simplest model of a thin screen placed between the source and the observer, it is easy to see that the method is insensitive to the location of the screen.

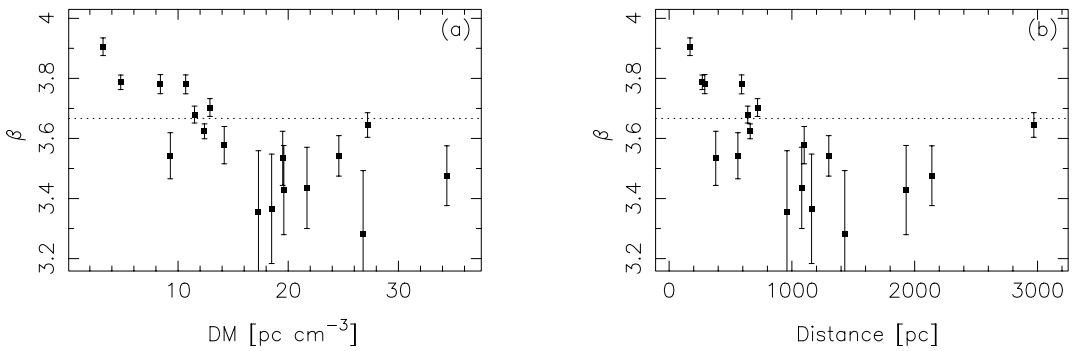

FIG. 3.—Values of β are plotted against (*a*) DM and (*b*) distance. For PSR B0823+26, PSR B0834+06, PSR B1133+16, and PSR B1919+21, $\langle\beta\rangle$ (the average of β from different observing sessions) is used. The dotted line indicates the Kolmogorov index 11/3. The uncertainties in values of β are at ± 1 σ levels.

2.3. *Persistent Drifting Features in Dynamic Spectra*

According to the theoretical models for RISS which consider the underlying density fluctuations to be a stochastic process, drift slopes of patterns are expected to vary randomly about a zero mean value over refractive timescales (cf. Rickett 1990). From the time series of measurements (see Fig. 4*a*–4*x* of Paper I), we see that this broad picture is substantiated by a number of pulsars, of which PSR B0823+26 and PSR B0919+06 form good examples. However, as mentioned earlier, our data also show several examples where the drifting features are "persistent" and do not show frequent sign reversals of slopes. A visual examination reveals that data from the first three observing sessions of PSR B0834+06 and from the two sessions of PSR B1919+21 form the best examples of such persistent slopes, as they are characterized by a complete absence or few epochs of slope reversals, e.g., PSR B0834+06(I), PSR B1919+21(II). A closer inspection of Figure 4 of Paper I (and also Fig. 2 of this paper) reveals that there are several other pulsars that form comparatively weaker examples of such a property; PSR B0329+54, PSR B0823+26(II), PSR B1540−06, PSR B2020+28, and PSR B2310+42 belong to this category.

To make a quantitative distinction between the two cases, viz., "frequent drift reversals" and "persistent drift slopes," we examine the distributions of the measured drift slopes for a clear "skewness" with respect to zero. Selected plots of such distributions are shown in Figures 4*a*–4*d*) to illustrate this scheme. The idea here is to identify data for which the mean drift slope, $\langle dt/dv \rangle$, is substantially offset from zero in comparison to its observed fluctuations. Data for which mean slopes are smaller than the rms fluctuation [$\langle dt/dv \rangle < \delta(dt/dv)$] and are free from a skewness in the distribution (e.g., Fig. 4*b*) are categorized as class I, and those with mean slopes offset from zero by more than the rms [$\langle dt/dv \rangle \gtrsim \delta(dt/dv)$] and have a skewed distribution (e.g., Figs. 4*a* and 4*c*) are labeled class II. The classification becomes ambiguous when the quantities $\langle dt/dv \rangle$ and $\delta(dt/dv)$ have substantial uncertainties, and the skewness is not well pronounced; these are labeled "NC" (nonclassifiable). Column (5) of Table 7 shows the "drift class" decided in this manner.

According to the above scheme, PSR B0834+06(I), PSR B0834+06(II), PSR B0834+06(III), PSR B1919+21(I), and PSR B1919+21(II) come under class II. For PSR B0329+54, PSR B0823+26(II), PSR B1133+16(III), PSR B1237+25, PSR B2045−16, and PSR B2310+42, the estimates of $\langle dt/dv \rangle$ and $\delta(dt/dv)$ are comparable, but the uncertainties are large; hence, we treat them as NC. The rest of the data are free from such ambiguities and belong to class I. A special pulsar in this context is PSR B0834+06, which shows the behavior of class I in the final observing session, much in contrast to what is seen in the first three sessions.

Earlier studies of dynamic spectra (Gupta et al. 1994) reported a similar property for PSR B0628−28 and PSR B1642−03. For PSR B0628−28, no persistent drifting features are seen in our data. As mentioned before, our observations show PSR B0834+06 changing the behavior from persistent drift slopes (1993 January–1994 June) to frequent slope reversals (1995 April–July). For PSR B1919+21, we do not have similar information, as it was not followed up for a third session. From these examples, it appears that persistent drifting features usually last over time intervals of the order of several months to a few years.

2.3.1. *Implications for the Density Spectrum*

We now examine the implications of our observations of persistent drift slopes for the nature of the density irregularity spectrum. The crucial question is whether the density structures responsible for such effects form part of the power-law spectrum determined by measurements of $\delta\theta_{\rm ref}$ and $\langle\theta_{\rm diff}\rangle$, as described in § 2.2.3. This can be answered by extrapolating the power-law spectrum to $\kappa = 1/S$ (where S corresponds to the time span over which persistent drift slopes are observed), estimating the expected rms refractive angle that would be produced by the power at these scales, and comparing this with the measured values of $\langle\theta_{\rm ref}\rangle$. The

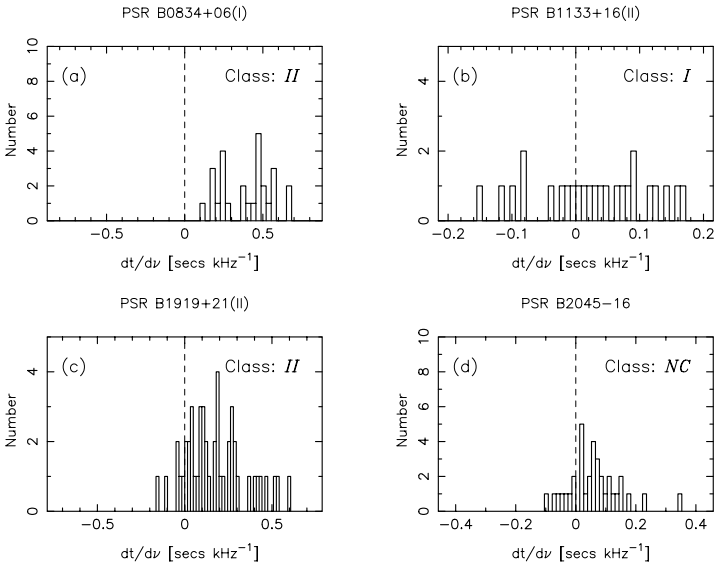

FIG. 4.—Sample plots of the histograms of drift rates (dt/dv) shown to illustrate the drift classification scheme. The pulsar name and session identification (wherever needed) are given at the top of each panel, and the drift class is given at the top right corner of the panel. The dashed vertical line corresponds to the zero drift rate.

expected rms refractive angle can be obtained simply by inverting equation (15), while using $U = (S/s_0)^{1/2}$ in place of u. Since $\langle\beta\rangle \approx 11/3$ for both PSR B0834+06 and PSR B1919+21, this gives $\delta\theta_{r,\mathrm{Kol}} = \langle\theta_{\mathrm{diff}}\rangle U^{-1/3}$. These values are given in column (7) of Table 9. Since the measured values of $\langle\theta_{\mathrm{ref}}\rangle$ for individual sessions are $\sim$1.2–2.7 times larger than the $\delta\theta_{r,\mathrm{Kol}}$ values, the probability of the density structures being part of a Kolmogorov-like spectrum is *rather low* ($\sim$1%–3% for PSR B0834+06 and $\sim$15%–20% for PSR B1919+21). Using the larger values of S for the combined data from multiple sessions increases the discrepancy with the measured $\delta\theta_{r,\mathrm{Kol}}$ ($\langle\theta_{\mathrm{ref}}\rangle$ is 3.4 times larger for PSR B0834+06 and 1.8 times larger for PSR B1919+21) and further reduces the probability of the structures being part of the power-law spectrum determined by $\delta\theta_{\mathrm{ref}}$ and $\langle\theta_{\mathrm{diff}}\rangle$ (0.1% for PSR B0834+06 and 6% for PSR B1919+21).

In Figures 5*a* and 5*b*, we have plotted the power levels at wavenumbers corresponding to diffractive and refractive scales (s_{diff} and s_{ref}), and at the larger spatial scales (S). The power levels at $\kappa = 1/S$ are significantly above the Kolmogorov expectations, which can be interpreted in different ways. One possibility is that a single power-law description is inadequate and the spectrum steepens at lower wavenumbers (10^{-14} m$^{-1} \lesssim \kappa \lesssim 10^{-11}$ m^{-1}). This would correspond to the type IIIA spectrum of § 1. From the estimated power levels, we find the average slope over this range ($\langle\beta_{\mathrm{steep}}\rangle$) to be much larger than 11/3 ($\approx$4.9 for PSR B0834+06 and $\approx$4.5 for PSR B1919+21). Such a "piecewise power-law" form of spectrum for representing the density fluctuations over a wide range of spatial scales (about 6 orders of magnitude or more) is an interesting possibility. The other possibility is that a Kolmogorov-like distribution of irregularities is superposed on a separate large-scale component giving rise to a "bump" near $\kappa \sim 10^{-13}$ to 10^{-12} m^{-1} (type IIIB spectrum of § 1). With the present observational data, it is difficult to discriminate between these two options.

2.3.2. *Constraints on Discrete Plasma Structures*

A possible alternative interpretation of the persistent drifting features is the existence of large-scale deterministic density structures along the line of sight to the pulsar. Our observations allow us to put constraints on the characteristics of such structures, in particular their sizes and electron densities. If we consider a refractive wedge with thickness L

TABLE 9

CONSTRAINTS ON THE CHARACTERISTICS OF HIGH-DENSITY CLOUDS

Data (1)	$\langle\theta_{\mathrm{ref}}\rangle$ (mas) (2)	$\langle V_{\mathrm{iss},c}\rangle$ (km s^{-1}) (3)	T_{sp} (days) (4)	N_e (cm^{-3}) (5)	S^{a} (AU) (6)	$\delta\theta_{\mathrm{r,Kol}}$ (mas) (7)
PSR B0834+06(I).....	0.24±0.01	217	120	3.6	15	0.09
PSR B0834+06(II).....	0.25±0.02	228	75	3.7	10	0.11
PSR B0834+06(III).....	0.23±0.01	270	75	3.4	12	0.11
PSR B0834+06[b]	0.24	238	500	3.6	70	0.07
PSR B1919+21(I).....	0.20±0.01	160	60	2.9	6	0.13
PSR B1919+21(II).....	0.12±0.01	226	90	1.8	12	0.10
PSR B1919+21[b]	0.16	193	350	2.3	40	0.09

[a] Lower limit on the spatial length scale.
[b] Combined data from the observing sessions given above.

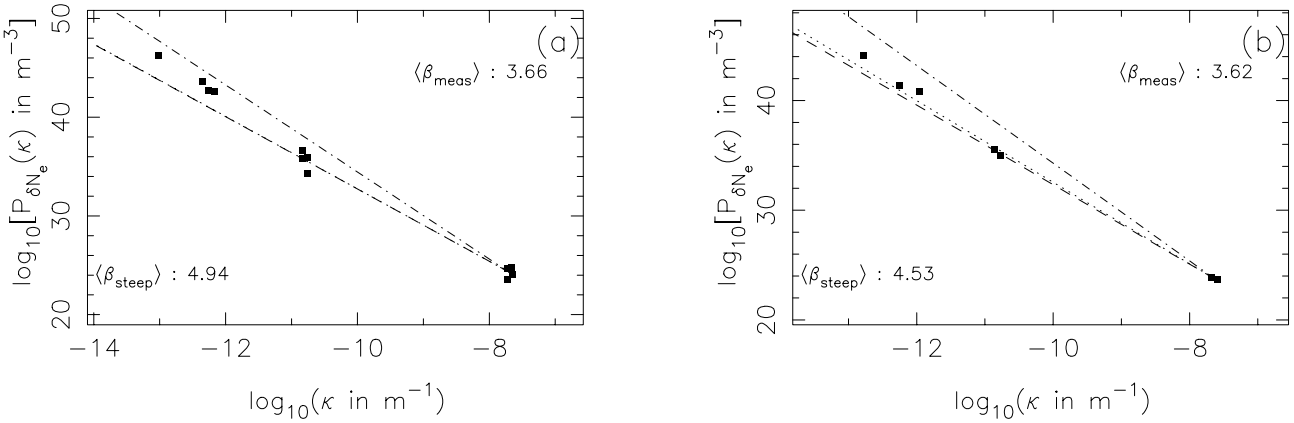

FIG. 5.— Composite density spectrum for (*a*) PSR B0834+06 and (*b*) PSR B1919+21. The dotted line represents the Kolmogorov ($\alpha = 11/3$) scaling, and the dot-dashed line $\alpha = 4$. The dashed line corresponds to the average slope ($\langle\beta_{\mathrm{meas}}\rangle$) determined by power levels at diffractive ($\sim 10^{-8}$ m^{-1}) and refractive ($\sim 10^{-11}$ m^{-1}) wavenumbers; this is given at the top right corner of each panel. For PSR B0834+06, $\langle\beta_{\mathrm{meas}}\rangle = 3.66$, which makes the dashed line coincide with the dotted one. The quantity given at the bottom left corner in (*a*) and (*b*) is the average slope ($\langle\beta_{\mathrm{steep}}\rangle$) over the wavenumber range determined by persistent drifts and refractive length scales.

and electron density N_e, the resulting refractive angle $\Theta_{\rm ref}$ is given by

$$\Theta_{\rm ref} = \frac{1}{k}\left(\frac{\partial\phi}{\partial r}\right) = \left(\frac{r_e\lambda_{\rm obs}}{k}\right)\int_0^L \frac{\partial N_e}{\partial r}\,dr\ . \qquad (16)$$

Under the assumption that N_e is uniform within the wedge, the integral simplifies to $\Delta N_e L/S$, where ΔN_e is the deviation from the ambient mean density (i.e., $\Delta N_e = N_e - \langle n_e\rangle$) and S is the transverse extent of the wedge. In the simplest case of a spherical cloud, the "aspect ratio" is unity ($S \sim L$), and assuming high electron densities ($N_e \gg \langle n_e\rangle$), the above expression simplifies to

$$\Theta_{\rm ref} = \frac{r_e\lambda_{\rm obs}^2 N_e}{2\pi}\ , \qquad (17)$$

where r_e is the classical electron radius (2.82×10^{-15} m) and $\lambda_{\rm obs}$ is the observing wavelength. We essentially estimate the electron density (N_e) required to produce the mean refractive angle, $\langle\theta_{\rm ref}\rangle$. The constraint on the size (S) is simply given by

$$S \gtrsim \langle V_{{\rm iss},c}\rangle T_{\rm sp}\ , \qquad (18)$$

where $T_{\rm sp}$ is the time span of observation over which drifting features lasted (col. [4] of Table 9), and $V_{{\rm iss},c}$ (i.e., $V_{\rm iss}$ computed using v_{d_c} and τ_d) is given by equation (12) (col. [3] of Table 9). The inferred values of N_e and S are estimated for PSR B0834+06 and PSR B1919+21, and are listed in columns (5) and (6) of Table 9.

The mean refractive angles required to produce the persistent drifting features seen in our data are moderate (0.1–0.3 mas). The important implication is that high electron densities ($N_e \sim 2$–$4\ {\rm cm}^{-3}$) need to persist over spatial scales much larger than the characteristic refractive scales ($S \gg s_{\rm ref}$) in order to give rise to such effects. Constraints on the size of these structures from a single observing session ($T_{\rm sp} \sim 100$ days) are $S \sim 10$ AU. Further, both these pulsars show similar persistent drifting features for more than one session. If we assume that the persistent drifts are sustained during the intervals between the successive sessions, then $T_{\rm sp}$ is much longer ($\sim$300–500 days), and the inferred sizes are $\sim$70 AU for PSR B0834+06 and $\sim$40 AU for PSR B1919+21 (see Table 9).

3. DISCUSSION

We have studied the properties of DISS and RISS for a number of nearby pulsars in an attempt to constrain the power spectrum of plasma density fluctuations in the ISM. We have focused on the results from two important and easily observable effects due to refractive scintillation: (1) modulations of DISS observables (v_d and τ_d) and flux density and (2) drifting bands in dynamic spectra. Our sample consists of mostly nearby pulsars ($D \lesssim 1$ kpc), and there is a reasonably uniform coverage in (l, b), DM, and D—hence, a more or less unbiased sample. Our data are sensitive to the density inhomogeneities in the spatial scale range $\sim10^7$–10^{13} m. Since all the basic measurements of DISS (v_d and τ_d) and RISS (dt/dv, m_b, m_t, and m_r) used in our analysis are from self-consistent data sets, the possibility of an observational bias is reduced. Furthermore, we have relied upon the more meaningful quantity, $\delta\theta_{\rm ref}/\langle\theta_{\rm diff}\rangle$, for discriminating between different kinds of density spectra and estimating β-values, compared to the earlier attempts, which often employed estimates of $\theta_{\rm ref}/\theta_{\rm diff}$ from one (or a few) epoch(s) of observations. As discussed in Paper I, it has also become possible from our observations to estimate the average scintillation properties more robustly than previously published work. Therefore, we believe the implications of our results for the nature of the electron density spectrum need serious consideration.

3.1. *Implications of the Main Results for the Density Spectrum*

The main results from our data can be summarized as follows:

1. Our observations show large-amplitude modulations of decorrelation bandwidth (v_d), scintillation timescale (τ_d) and flux density (F). The measured depths of modulations are found to be considerably larger than the predictions of a thin-screen model with a simple Kolmogorov form of density spectrum (hypothesis IA of § 1). Barring some cases, the measured modulation indices of v_d and F are consistent with $4 < \alpha < 4.3$, and those of τ_d with $11/3 < \alpha < 4.3$, as far as the predictions of a thin-screen model are concerned. For the flux modulation indices, better agreement is seen with spectra of type IA if the scattering medium is taken to be uniformly distributed along the line of sight. Even then, roughly half the measurements are significantly larger than the predictions of a type IA spectrum.

2. Measurements of refractive and diffractive angles are consistent with $\alpha < 4$, as the ratio $\delta\theta_{\rm ref}/\langle\theta_{\rm diff}\rangle$ is found to be below unity for all pulsars. Further, our estimates of density spectral slope (β) range from 3.3 to 3.9. While 18 of the 25 measurements are consistent with the Kolmogorov index (at $\pm$ 2 σ levels), for six pulsars ($D \sim$ 200–700 pc), β is found to be significantly larger than 11/3.

3. Persistent drifting bands lasting over many months are seen with PSR B0834+06 and PSR B1919+21, which imply excess power at spatial scales $\sim$10–100 AU (much larger than the refractive scales) compared to the expectations from a type IA spectrum. This is possible if the spectrum (1) is a piecewise power law that steepens at $\kappa < \kappa_{\rm ref}$ or (2) has a low wavenumber enhancement (hypotheses IIIA and IIIB, respectively, of § 1). An alternative possibility is the existence of localized density structures of spatial scales $\sim$10–70 AU and $N_e \sim 2$–$4\ {\rm cm}^{-3}$ (hypothesis IV of § 1).

3.1.1. *Refractive Modulations and Slopes of the Density Spectrum*

It is difficult to reconcile the first two results with a simple power-law model for the electron density spectrum in the ISM. Hence we look at them more critically.

Starting with the first result, we note that ours are not the first reported measurements of modulation indices larger than the Kolmogorov expectations. Flux monitoring observations were made earlier by a number of groups (Stinebring & Condon 1990; Kaspi & Stinebring 1992; Gupta et al. 1993; LaBrecque et al. 1994; Gupta et al. 1994). In Table 10 we summarize the results from all these observations, for pulsars common to our observations. To compare the measurements made at different frequencies, we use equation (4) for scaling the predicted modulation indices. We find that our measured flux modulation indices (col. [3]) are comparable to observations at nearby frequencies (e.g., cols. [4], [5], [8], and [9]). Further, most of the modulation indices given in Table 10 are significantly

TABLE 10

FLUX MODULATION INDICES FROM THE LITERATURE

NUMBER (1)	PULSAR (2)	ORT[a] (327 MHz) (3)	GRL94[b] (408 MHz) (4)	LRC93[c] (408 MHz) (5)	GRC93[d] (74 MHz) (6)	KS92[e] (610 MHz) (7)	SC90[f] (310 MHz) (8)	SC90[f] (416 MHz) (9)	SC90[f] (750 MHz) (10)
1	PSR B0329+54	0.23	0.40	...	>0.15	0.39	...	...	...
2	PSR B0628−28	0.30	0.33	...	...	...	...	...	...
3	PSR B0823+26	0.40	0.22	$\lesssim$0.45	>0.16	...	...	...	...
4	PSR B0834+06	0.40	0.53	$\lesssim$0.36	0.16	...	...	...	...
5	PSR B1133+16	0.30	...	...	0.18	...	...	...	...
6	PSR B1237+25	0.69	...	...	0.30	...	...	...	...
7	PSR B1508+55	0.24	...	...	0.28	>0.11	0.24	0.25	0.33
8	PSR B1604−00	0.47	...	$\lesssim$0.71	...	...	0.43	1.04	1.06
9	PSR B1919+21	0.47	...	...	>0.21	...	0.69	0.80	0.97
10	PSR B2016+28	0.40	0.25	...	...	...	0.18	0.21	0.35
11	PSR B2020+28	0.57	...	$\lesssim$0.36	...	...	0.38	0.53	0.50
12	PSR B2045−16	0.42	...	...	...	...	0.60	0.81	1.23

NOTE.—The frequency of observation is given in parentheses..

[a] Measurements from our data.

[b] Gupta, Rickett, & Lyne 1994.

[c] LaBrecque, Rankin, & Cordes 1994.

[d] Gupta, Rickett, & Coles 1993.

[e] Kaspi & Stinebring 1992.

[f] Stinebring & Condon 1990.

larger than those expected from a Kolmogorov spectrum (type IA of § 1). For modulation indices of v_d and τ_d, there are very few observations reported in the literature that we are aware of. Gupta et al. (1994) have reported v_d modulation indices for six pulsars from their long-term scintillation study at 408 MHz (their Table 4). The values for the five pulsars common to our observations are comparable, and more than the predicted values for type IA spectra.

As discussed in § 2.1.3, if the scattering medium is assumed to be uniformly distributed along the line of sight, our results of flux modulation indices are in somewhat better agreement with a type IA spectrum. About half the values are then consistent with $\alpha = 11/3$, and the remaining half are consistent with $11/3 < \alpha < 4$. Because of the lack of relevant predictions, similar comparisons cannot be made for the modulations of v_d and τ_d. Thus our results from modulation indices can be partially reconciled with our β estimates.

Turning now to the second result, we note that it may be possible that our refractive angle measurements (and hence the β-values derived from them) underestimate their true values, despite the first-order correction applied for the effect due to the alignment angle ψ ($\delta\Theta_{\rm ref} = \sqrt{2}\delta\theta_{\rm ref}$). The underlying assumption of random fluctuations of $\Theta_{\rm ref}$ and ψ need not be true always, in which case the above correction may still be inadequate. Observations of persistent drifts (for two pulsars) and statistically significant nonzero values of $\langle\theta_{\rm ref}\rangle$ (for five pulsars) in our data indicate that such situations exist in practice. In such cases, the true β-values can be larger than our estimates, thereby reducing the disagreement with the first result.

Another aspect worth mentioning is the assumption of isotropic turbulence in the ISM. It is known that the presence of a strong magnetic field will make the turbulence highly anisotropic (Higdon 1984, 1986), a concept well supported by the recent observations of field-aligned anisotropic density structures in the inner solar wind (Armstrong et al. 1990; Anantharamaiah, Gothoskar, & Cornwell 1994). However, it is unclear at present what is the importance of anisotropy in the ISM. As Coles et al. (1987) point out, there may be several important consequences for ISS in the case of anisotropic turbulence, but they have not been worked out analytically. The anisotropic turbulence will make C_n^2 sensitive to the field geometry and can also affect the inner scale cutoff; hence, it can potentially influence the modulations of DISS observables and flux. Since the fluctuations in the large-scale Galactic magnetic fields have length scales $\sim$100 pc (Simonetti, Cordes, & Spangler 1984), anisotropic ISS is probably more relevant for nearby pulsars. Furthermore, there is evidence for large-scale ($\sim$100–500 pc) spatial inhomogeneities in C_n^2 within the local ($\lesssim$1 kpc) ISM (Bhat et al. 1997, 1998a). Therefore, anisotropic ISS may be relevant for some of our pulsars.

3.1.2. *Persistent Drift Slopes and Multiple Imaging Events*

In addition to persistent drifting bands, phenomena such as multiple imaging events (e.g., Wolszczan & Cordes 1987) and extreme scattering events (ESEs; see, e.g., Fiedler et al. 1987) are also thought to be caused by large-scale deterministic density structures in the ISM. While ESEs are mostly observed with compact extragalactic radio (EGR) sources, the other two effects are seen in pulsar dynamic spectra. So far, multiple imaging events have been reported for seven pulsars (Hewish et al. 1985 for PSR B1133+16 and PSR B1642−03; Cordes & Wolszczan 1986 for PSR B0919+06, PSR B1133+16, and PSR B1919+21; Wolszczan & Cordes 1987 for PSR B1237+25; Kuz'min 1992 for PSR B1919+21; Gupta et al. 1994 for PSR B2016+28; Rickett, Lyne, & Gupta 1997 for PSR B0834+06; Bhat et al. 1998b for PSR B1133+16). Very few observations of persistent drifts have been reported so far. For PSR B0834+06 and PSR B1919+21, our data show persistent drift slopes lasting over $\sim$300–500 days. A similar property is reported by Gupta et al. (1994) for PSR B0628−28 and PSR B1642−03, and Smith & Wright (1985) see some signatures of it for PSR B0823+26 and PSR B1929+10. PSR B1937+21 is the only pulsar for which the occurrence of ESEs has been reported. To date, a total of 10 ESEs have

been identified with EGR sources (see Fiedler et al. 1994 for a summary).

Fiedler et al. (1987) infer a very high density cloud ($N_e \sim 1000$ cm^{-3}) of ~ 7 AU from the observations of ESEs in the light curves (at 2.7 and 8.1 GHz) of quasar 0954+658. This unusually large constraint on the density can, however, be relaxed to $N_e \sim 100$ cm^{-3} if one considers an edge-on geometry with an aspect ratio (η) of 10:1. Cognard et al. (1993) infer clouds of similar densities ($N_e \sim 25$–220 cm^{-3}) from the ESE observed for PSR B1937+21 at 1.4 GHz. However, the requirement on the size is much smaller (~ 0.05–0.1 AU), as the event spans only a short period of 15 days. Rickett et al. (1997) suggest a structure of ~ 3 AU and $N_e \sim 40$ cm^{-3} (for $\eta = 1$) as one of the possible scenarios to explain the interstellar fringes observed at 408 MHz for PSR B0834+06. Compared to all these results, the structures inferred from our data are larger in size but relatively less dense.

The similarity in the interpretations of the above three effects indicates a probable connection between them. Romani, Blandford & Cordes (1987) point out that the periodicities in pulsar dynamic spectra, the LFV of quasars, and the ESE of 0954+658 (Fiedler et al. 1987) can be understood in terms of multiple imaging and focusing by large-scale refracting structures in the ISM. It is interesting to note that PSR B0834+06 and PSR B1919+21, which show persistent drifts in our observations, are known to have shown multiple imaging events (Cordes & Wolszczan 1986; Kuz'min 1992; Rickett et al. 1997). Similarly, PSR B1133+16, which shows evidence for multiple imaging in our data (see also Hewish et al. 1985; Cordes & Wolszczan 1986), also shows some signatures of persistent drifts lasting over several weeks (see Figs. 2*j* and 2*k*). The large proper motion of this pulsar (≈ 475 km s^{-1}) would imply that the corresponding spatial scales are ~ 10 AU, quite comparable to the size of the density structures inferred from the persistent drifts of PSR B0834+06 and PSR B1919+21 (see Table 9). Thus, our observations of these three pulsars along with detections of multiple imaging events in earlier observations form direct evidence in favor of the connection between the two effects, thereby supporting the view of Romani et al. (1987) on scattering effects due to localized high-density structures. It is not clear whether there is a large population of such structures in the Galaxy, but the observational data suggest that hypothesis IV is relevant at least for some lines of sight.

3.2. *A Summary of Various Constraints on the Plasma Density Spectrum*

A number of attempts have been made in the recent past toward determining the form of the density spectrum, and there are conflicting interpretations from various kinds of measurements. While several observations are consistent with a simple Kolmogorov form (hypothesis IA), there is a substantial amount of observational data that go against it. Attempts have also been made to construct a composite spectrum extending over a wide range of spatial scales. Here we give an overview of various observational evidence accumulated so far, from our data as well as from the published literature.

Among the several possible alternatives to the *pure* Kolmogorov form (hypothesis IA), three specific cases, viz., (1) steeper spectra (hypothesis II), (2) a Kolmogorov spectrum truncated at a large inner scale (hypothesis IB), and (3) a Kolmogorov spectrum with a low wavenumber enhancement (hypothesis IIIB) have been more commonly discussed in the literature. Effects due to such *non-Kolmogorov* forms of spectra are not fully understood yet. Something that is common to all three is that they are of a more refractive nature than case IA. Most observational evidence against hypothesis IA can therefore be interpreted in terms of one or more of the remaining possibilities. In § 3.2.1 we describe the observational evidence in support of a pure Kolmogorov form, and in § 3.2.2 we summarize the observational data that go against it. In § 3.2.3 we attempt to reconcile the various observational results and discuss the possible implications for the overall nature of the density spectrum.

3.2.1. *Evidence in Favor of a Kolmogorov ($\alpha = 11/3$) Spectrum*

Our observations show that the measurements of diffractive and refractive angles, and consequently the slope parameter (β) derived from them, are consistent with a Kolmogorov form of spectrum (hypothesis IA of § 1) for a large number (14 out of 18) of pulsars. A quite similar result is reported by Smith & Wright (1985), where the measured scattering angles are found to be compatible with a Kolmogorov spectrum extending over a range of spatial scales from $\sim 10^9$ to $\sim 10^{12}$ m. There are 14 pulsars common to our sample and that of Smith & Wright (1985). While we find five pulsars with β significantly larger than 11/3 (see Table 8), the sample of Smith & Wright (1985) has three pulsars favoring $11/3 < \alpha < 4$ (see their Table 1). PSR B1929+10 is an interesting case for which a steeper spectrum is suggested by both the observations ($\beta \approx 3.91 \pm 0.03$ from our data and $\theta_{\rm ref}/\theta_{\rm diff} \approx 0.61$ from Smith & Wright 1985). Among the remaining four pulsars, PSR B0834+06 is a special case with β larger than 11/3 in session II (note that $\langle\beta\rangle \approx 3.69 \pm 0.03$). For PSR B1133+16 and PSR B1604−00, no meaningful drift measurements were made by Smith & Wright (1985). Thus, in general, measurements of drift slopes in dynamic spectra support an $\alpha \approx 11/3$ spectrum over the spatial scale range $\sim 10^7$–10^{12} m.

The scaling of scintillation parameters with the frequency and/or distance is known to be sensitive to α. Although there is ambiguity involved in relating the scaling exponent to α, it can be resolved using other observational indicators. Cordes et al. (1985) find the frequency scaling of decorrelation bandwidths (for five pulsars) to be consistent with the index $\alpha = 3.63 \pm 0.2$. For the common pulsar PSR B0329+54, we find $\beta \approx 3.3 \pm 0.2$, consistent with the result of Cordes et al. (1985). Another piece of evidence in this direction comes from the scaling of the decorrelation bandwidth and the scintillation timescale for PSR B1937+21 (Cordes et al. 1990), where the scaling implies $\alpha = 3.55 \pm 0.11$. Further evidence in support of a Kolmogorov form comes from the VLBI observations. Gwinn et al. (1988b) studied the image wander of clusters of H_2O masers in W49 and Sgr B2 and showed $\alpha \approx 3.67$ up to length scales $\sim 10^{11}$ m. Observations of the scattering disk of the pulsar PSR B1933+16 are found to be consistent with $\alpha = 3.52 \pm 0.13$ at length scales of 10^6–10^7 m (Gwinn et al. 1988a).

3.2.2. *Evidence in Favor of Non-Kolmogorov Forms of Spectra*

Evidence against a simple Kolmogorov form comes from a number of observations. Many pulsars are known to show flux modulations well in excess of the Kolmogorov predic-

tions (see § 3.1.1 for a discussion and summary). Although an immediate interpretation is that the spectrum needs to be steeper (hypothesis II of § 1), a Kolmogorov spectrum truncated at a sufficiently large inner scale (hypothesis IB of § 1) can also explain large flux modulations (cf. Coles et al. 1987; Goodman et al. 1987). Similarly, measurements of modulation indices of v_d and τ_d are found to be significantly larger than the Kolmogorov predictions for almost all pulsars (see § 3.1.1) but are consistent with the predictions for $11/3 < \alpha < 4.3$ given by Romani et al. (1986).

Further evidence favoring a *non-Kolmogorov* form of spectrum comes from measurements of angular broadening and studies of long-term DM variability. Using the first method, Spangler & Cordes (1988) measure $\alpha = 3.79 \pm 0.05$ toward the compact source 2013+370, and Wilkinson, Spencer, & Nelson (1988) obtain $\alpha = 3.85 \pm 0.05$ toward Cygnus X-3. Phillips & Wolszczan (1991) studied DM variations of PSR B0823+26, PSR B0834+06, and PSR B0919+06 over a time span ~ 2 yr, and their structure function analysis shows α to be larger than 11/3 ($\langle \alpha \rangle = 3.84 \pm 0.02$) over the spatial scale range $\sim 10^7$–10^{13} m. At first sight, this might appear contrary to our observations, since we find the β-values for these pulsars to be consistent with 11/3 within the errors (Table 8). It is important to note that our β-values are sensitive to fluctuations on spatial scales $\sim 10^7$–10^{11} m, whereas the DM fluctuations probe $\sim 10^{11}$–10^{13} m. As mentioned in § 2.3.1, from persistent drifting features observed in our PSR B0834+06 data, we infer a similar enhancement in power level at spatial scales $\sim 10^{12}$–10^{14} m compared to the Kolmogorov expectations (see Fig. 5*a*).

Backer et al. (1993) studied DM variations of four pulsars (PSR B1821−24, PSR B1855+09, PSR B1937+21, and PSR B1951+32) spanning the DM range 13–119 pc cm^{-3}. They find the δDM-DM relation to be much flatter than that expected based on DISS, which they interpret as an evidence against a direct link between the density fluctuations responsible for DM variations and those which cause DISS. They suggest a model comprising several wedgelike structures randomly distributed along the line of sight to account for the observed DM variations. It may be mentioned that Rickett et al. (1997) suggest a similar explanation for the fringing event seen in the PSR B0834+06 data at 408 MHz. In both cases, the models proposed for the density fluctuations are in accordance with hypothesis IV of § 1.

Observations of unusual scattering phenomena such as ESEs, multiple imaging events, and persistent drifting features can be considered to be a strong evidence in favor of non-Kolmogorov forms of spectra. Multiple imaging events are expected to be rare for type IA spectra, but can be more common if the spectrum is type II with $\alpha \gtrsim 4$ (Hewish et al. 1985; Rickett 1990). But the existing observational data are not adequate to make a firm statement on the statistics of their occurrence. The more commonly favored explanation is in terms of refraction through discrete structures (e.g., Cordes & Wolszczan 1986). Observations of ESEs are also explained in terms of large-scale refractors (~ 10 AU) in the ISM (Romani et al. 1987; Fiedler et al. 1994; Clegg, Fey, & Lazio 1998). As discussed in § 2.3.2, persistent drifting bands can also be understood in terms of discrete density structures in the ISM. Relatively rare occurrences of the three effects indicate that these density structures are localized. As stated in § 3.1.2, there is some evidence for the connection between these effects; for example, three of our pulsars, PSR B0834+06, PSR B1133+16, and PSR B1919+21, are known to have shown both multiple imaging and persistent drifts. Thus the data accumulated so far clearly signify the importance of discrete structures in the ISM, thereby supporting hypothesis IV, at least along some lines of sight.

3.2.3. *Overall Nature of the Density Spectrum in the Local* (1 kpc) *ISM*

Various methods discussed in §§ 3.2.1 and 3.2.2 probe different parts of the density fluctuation spectrum, and it is interesting to see that the measurements based on a particular method have similar implications for the nature of the spectrum. It is worth examining to what extent these observational results can be reconciled and what they mean for the overall nature of the spectrum. The frequency scaling of v_d basically probes spatial scales in the range $\sim 10^6$–10^8 m, where α is found to be consistent with 11/3. VLBI angular broadening of PSR B1933+16 also probes a similar range ($\sim 10^6$–10^7 m), and the value of α inferred from this is also consistent with 11/3. The measurements of drift slopes probe spatial scales near $\sim 10^{10}$–10^{11} m, and support an $\alpha \approx 11/3$ spectrum toward a number of lines of sight. Further, observations of image wander of H_2O masers, which also probe spatial scales of similar range ($\sim 10^{11}$ m), give another piece of independent evidence for an $\alpha = 11/3$ spectrum. Thus the density spectrum seems to be a power law with the Kolmogorov index (hypothesis IA) in the range $\sim 10^6$–10^{11} m.

Long-term DM variability, as reported by Phillips & Wolszczan (1991), probes much larger spatial scales ($\sim 10^{11}$–10^{13} m), and the results indicate that the strength of density fluctuations at these scales is significantly larger than the Kolmogorov expectations. As discussed in § 2.3.1, persistent drift slopes observed in our data are also suggestive of excess power at $\sim 10^{12}$–10^{13} m. These, combined with the results for smaller spatial scales ($\sim 10^6$ to $\sim 10^{11}$ m) would warrant a "multicomponent" spectrum (i.e., hypothesis III of § 1) in the range $\sim 10^6$–10^{13} m, with either a break near $\kappa \sim 10^{-11}$ m^{-1} (type IIIA) or a "bump" at $\kappa \sim 10^{-12}$ to 10^{-13} m^{-1} (type IIIB).

The modulations of DISS observables (v_d and τ_d) and flux, which are indicative of the strength of density fluctuations near refractive scales ($\sim 10^{10}$–10^{11} m), are not in agreement with the Kolmogorov predictions (§§ 2.1, 3.1). However, the implications for the density spectrum here are not unambiguous, since the observed discrepancies can, at least partly, be attributed to the inadequacies of the thin-screen models. The thin screen is not likely to be a valid approximation toward most pulsars within 1 kpc, and the theoretical treatments need to be refined to analyze the perturbations of DISS parameters due to extended and/or inhomogeneous media. Hence the modulation indices of observables, although discrepant with the predictions of a type IA spectrum, do not put stringent constraints on the form of the spectrum. The results from angular broadening measurements (toward Cyg X-3 and 2013+270) and DM variations of Backer et al. (1993) are also not in direct contradiction to the implications from other measurements. The lines of sight of Cyg X-3 and 2013+270 can be treated as atypical, since they are characterized by exceedingly large strengths of scattering, predominantly from the region beyond ~ 1 kpc. The conclusion of Backer et al. (1993)—that wedgelike discrete structures are responsible for DM

variations—is largely based on observations of distant ($D \gtrsim 1$ kpc) pulsars.

Observations such as ESEs, multiple imaging, and persistent drifts can be interpreted in terms of discrete density structures in the ISM (hypothesis IV of § 1). Multiple imaging events have been reported only for seven pulsars, and four pulsars are known to have shown persistent drift slopes (§ 3.1.2). To date, ESEs have been identified in the data of nine radio sources and one pulsar. The existing observational data therefore suggest that such effects are relatively rare phenomena, which means discrete structures may *not* be *very* common. Hence hypothesis IV (i.e., a density spectrum of irregularities with superposed deterministic structures) seems to be relevant only for a limited number of lines of sight. The overall picture emerging from the above discussion is that underlying density fluctuations can, in general, be described by hypothesis III (i.e., a Kolmogorov-like spectrum which either steepens or exhibits a "bump" in the low wavenumber range), and hypothesis IV applies to some specific lines of sight.

3.3. *Implications for the Theoretical Models*

The simplest scenario usually considered by the theoretical models is of a thin-screen scattering geometry and a density irregularity spectrum of type IA (i.e., $s_{\rm inn} \ll s_{\rm diff}$, $s_{\rm out} \gg s_{\rm ref}$). Although the estimates of density spectral slope (β) from our data are consistent with $11/3 \lesssim \alpha < 4$, the corresponding theoretical predictions for the modulation indices of v_d, τ_d, and F do not match the observations. This inconsistency gives a clear indication of the inadequacy of theoretical models based on such a simple scenario.

Not many investigations have been made so far to understand refractive scintillation effects due to more complex but realistic scenarios such as an extended scattering medium. Nevertheless, a partial reconciliation of our results is possible if we consider a geometry with the scattering material uniformly distributed along the line of sight. Such a scenario in combination with $11/3 \leq \alpha < 4$ will suffice to account for the measured flux modulation indices from our data. If such models can also give rise to ~ 2 times larger modulations of v_d and τ_d compared to the thin-screen model, then it is possible to reconcile the observed modulations of all three quantities and estimates of the slope with $11/3 \leq \alpha < 4$ (i.e., type IA and II spectra). At present, theories for extended media—homogeneous and/or inhomogeneous—are not fully developed, but detailed treatments have become necessary in the light of new results from our observations.

Alternatives such as models based on hypothesis IB (say, with $s_{\rm ref} > s_{\rm inn} > s_{\rm diff}$) deserve some consideration here, as they can give rise to some observable effects akin to those produced by type II spectra. For example, such models can give rise to large modulations of flux and periodic patterns in dynamic spectra (cf. Goodman et al. 1987; Coles et al. 1987). However, at present, there is no compelling observational evidence suggesting a large inner scale. Furthermore, it is unclear whether such models can also give rise to large modulations of v_d and τ_d, and still be consistent with $11/3 \leq \beta < 4$. In this context, models based on hypotheses IIIA and IIIB also need to be examined critically.

In addition to general phenomena such as modulations of DISS observables and flux density, and drifting bands in dynamic spectra, a satisfactory model also needs to account for relatively rare phenomena such as persistent drifts, multiple imaging events, and extreme scattering events. All three effects can be understood in terms of refractive effects due to large-scale deterministic structures (i.e., hypothesis IV of § 1), suggesting that an interconnection between them is likely. Despite the progress made so far, we still lack quantitative interpretations describing these phenomena, and further investigations are needed.

4. CONCLUSIONS

We have attempted to constrain the power spectrum of plasma density fluctuations in the ISM by studying refractive effects in pulsar scintillation. We have used the data from a long-term scintillation study of 18 pulsars. Reliable and accurate estimates of diffractive and refractive scintillation properties were obtained by monitoring the dynamic scintillation spectra at a number of epochs spanning several months. We studied two important and easily observable effects due to refractive scintillation: (1) modulations of scintillation observables and flux density and (2) drifting bands in dynamic spectra, which provide two independent means of constraining the form of the density irregularity spectrum. We have considered a set of hypotheses to describe the possible potential forms of the density spectrum and tested them using our data. The relevant hypotheses are (IA) $\alpha = 11/3$ (Kolmogorov spectrum), (IB) $\alpha = 11/3$ with large inner scale; (II) $\alpha > 11/3$ ("steep" spectrum); (IIIA) "piecewise" power law, (IIIB) power law with low wavenumber enhancement; and (IV) power law with superposed discrete structures. At present, quantitative predictions are available only for the cases covered under hypotheses IA and II. On comparing the observed modulation indices of diffractive scintillation observables—decorrelation bandwidth (v_d) and scintillation timescale (τ_d)—and pulsar flux density (F) with the predictions, we find that the measured values are considerably larger than the predicted values for a thin-screen model with a density spectrum of type IA. The measured modulation indices are spread over a wide range of values and are consistent with the predictions for power-law spectra with $11/3 < \alpha < 4.3$ (hypothesis II). The flux density modulations will also be consistent with a smaller range, $11/3 \leq \alpha < 4$, if an extended scattering geometry with uniformly distributed scattering material along the line of sight is considered. Predictions are not available for the modulations of v_d and τ_d for such a medium. Estimates of density spectral slope (β) are obtained from our measurements of diffractive and refractive scattering angles, and are found to be reasonably close to 11/3 (within the measurement uncertainties) for a number of pulsars (14 out of 18). For several nearby pulsars (distance $\sim$200–700 pc), β is found to be significantly larger than 11/3 (but less than 4). Thus, there are conflicting interpretations, and the results from the two methods are *not fully* reconcilable within the framework of theoretical models based on hypotheses IA and II. Further, the observations of persistent drifting bands lasting over many months seen in our data (e.g., PSR B0834+06 and PSR B1919+21) indicate that there is excess power at spatial scales $\sim$10–100 AU, much larger than the refractive scales. This would mean the spectrum either needs to be a piecewise power law or has a bump in the low wavenumber range (hypotheses IIIA and IIIB, respectively). An alternative interpretation is the existence of large-scale ($\sim$40–70 AU) high-density ($N_e \sim 2$–4 cm^{-3}) clouds along some lines of sight (hypothesis IV).

A careful consideration of all available results from the literature and our current work leads us to the picture of a Kolmogorov-like spectrum ($\alpha \approx 11/3$) in the wavenumber range $\sim 10^{-6}$ to $\sim 10^{-11}$ m^{-1}, which either steepens or has a bump of enhanced power at low wavenumbers ($\kappa \sim 10^{-12}$ to 10^{-13} m^{-1}). In addition, observations of relatively rare phenomena such as persistent drift slopes, ESEs, and multiple imaging events suggest the existence of localized high-density structures along some lines of sight. Thus the observational data indicate that the electron density fluctuations in the ISM can, in general, be described by hypothesis III, and hypothesis IV applies to some specific lines of sight. Unlike the case with hypotheses I and II, refractive scintillation effects due to scattering media described by hypotheses III and IV have not been fully developed. We hope the present work will stimulate detailed theoretical work necessary toward an improved understanding of refractive scintillation effects in pulsar signals and the power spectrum of plasma density fluctuations in the ISM.

The authors wish to thank J. Chengalur and M. Vivekanand for reading an earlier version of this manuscript and giving useful comments. We thank an anonymous referee for an illuminating review, which stimulated several lively discussions among us and also helped us in improving upon the clarity as well as the content of the paper.

APPENDIX A

STATISTICAL RELIABILITY OF THE DATA

The statistical quality of our data largely depends on the number of independent measurements ($N_{\rm ep}$) and the number of refractive cycles ($N_{\rm ref}$) spanned during the time span of observation. For the latter, we need to know the timescale of fluctuations of our observables. Expectations based on simple models are that the fluctuations of all three quantities—decorrelation bandwidth (v_d), scintillation timescale (τ_d), and flux density (F)—occur over refractive timescales ($\tau_{\rm ref}$), which are expected to be days to weeks at our observing frequency. A structure function analysis was attempted for determining the timescales but did not yield meaningful results owing to the limited number of measurements. However, since our measurements of decorrelation bandwidth and scintillation timescale are fairly accurate (with typical uncertainties $\sim$5%–10%), first-order estimates of refractive timescales can be estimated using the expression (Rickett 1990)

$$\tau_{\rm ref} \approx \left(\frac{2f_{\rm obs}}{v_d}\right)\tau_d \,, \tag{A1}$$

where $f_{\rm obs}$ is the observing frequency. The above relation is based on simple models, i.e., scattering due to a thin screen with a power-law form of density spectrum. We use the estimates of $v_{d,g}$ and $\tau_{d,g}$ obtained from the global ACF analysis (see Paper I) to estimate $\tau_{\rm ref}$. Our values of $\tau_{\rm ref}$ and $N_{\rm ref}$ (given by $T_{\rm sp}/\tau_{\rm ref}$, where $T_{\rm sp}$ is the time span of observation) are listed in columns (6) and (7) of Table 3. We do not have any pulsar for which the expected timescale of fluctuation is larger than the time span of observation.

On the basis of the estimates of $N_{\rm ref}$, the data are divided into three broad categories: (A) $N_{\rm ref} \geq 10$, (B) $N_{\rm ref} \sim 5$–10, and (C) $N_{\rm ref} < 5$. In a similar way, a categorization is made based on the number of measurements: (A) $N_{\rm ep} \geq 20$, (B) $N_{\rm ep} \sim$ 10–20, and (C) $N_{\rm ep} < 10$. These categories are listed in columns (8) and (9), respectively, of Table 3. The data that have "C" for either of the two categories are considered to be of poor statistical quality. These include PSR 1540−06, PSR 2016+28, and PSR 2310+42, which have only a few cycles of fluctuations (mainly due to their low space velocities), data from the initial session of PSR B1133+16 ($N_{\rm ep} = 6$) and PSR 1237+25, PSR 1508+55, and PSR 1929+10. From Table 3 we find seven data sets in category A (in terms of both $N_{\rm ep}$ and $N_{\rm ref}$), and 11 with reasonably good statistical reliability. These 18 data sets are used while comparing our results with the predictions.

APPENDIX B

NON-ISS CONTRIBUTIONS TO THE MODULATION INDICES

B1. MEASUREMENT NOISE

First of all, we consider the effect due to various sources of noise involved in the measurement process. These include (1) errors due to the Gaussian fitting done to the ACF ($\sigma_{\rm mod}$), relevant for v_d and τ_d; (2) "DISS noise" or estimation errors due to the finite number of scintles in the dynamic spectrum ($\sigma_{\rm est}$), relevant for v_d, τ_d, and F; and (3) errors due to the flux calibration ($\sigma_{\rm cal}$), relevant for F. The techniques for estimation of these quantities are discussed in detail in Paper I. The time series of v_d, τ_d, and F (see Figs. 4*a*–4*x* of Paper I) give some idea about these noise sources, where the uncertainties in v_d and τ_d are given by $(\sigma_{\rm mod}^2 + \sigma_{\rm est}^2)^{1/2}$ and that in F is given by $(\sigma_{\rm cal}^2 + \sigma_{\rm est}^2)^{1/2}$. The effect of these noise sources is an apparent increase in the modulations, and therefore the measured modulation indices (m_b, m_t, and m_r) need to be corrected for this. We estimate the noise modulation indices ($m_{\rm noise}$) as the typical fractional uncertainties of these quantities, and these are given in columns (3), (4), and (5) of Table 4. The measured modulation index ($m_{\rm meas}$) is then given by

$$(m_{\rm meas})^2 = (m_{\rm riss})^2 + (m_{\rm noise})^2 \,. \tag{B1}$$

The RISS-induced modulations ($m_{\rm riss}$) of v_d, τ_d, and F obtained in this manner are given in columns (6), (7), and (8) of Table 4. Since noise modulation indices are typically 0.1 for our data, their contributions to the measured modulation indices are

usually marginal. The only exceptions are τ_d modulations of PSR B0823+26(II) and PSR B1929+10, for which $m_{\rm noise}$ is slightly larger than the estimate of m_t, and the flux modulation of PSR B1133+16(I) with $m_{\rm noise} \approx m_r$. Note that the last two data are of poor statistics because of the limited number of measurements ($N_{\rm ep}$) as described earlier. Further, for part of the data of PSR B0834+06 (II and III) and PSR B2310+42, corrected estimates of m_t are significantly lower (<0.1) compared to their uncorrected values. Excluding these six measurements and the data with poor statistical reliability, global averages of modulation indices are $\langle m_b \rangle = 0.36$, $\langle m_t \rangle = 0.17$, and $\langle m_r \rangle = 0.44$, very close to those obtained from the direct measurements.

B2. EFFECT OF VARIABLE FARADAY ROTATION ON FLUX DENSITY MODULATION

Since the ORT is sensitive only to linearly polarized radiation with the electric field in the north-south plane, we need to consider the apparent flux modulation index due to epoch-to-epoch variations of Faraday rotation (due to the Earth's ionosphere). A significant fraction of radiation from most pulsars is known to be linearly polarized, and our sample consists of pulsars with fractional linear polarization (at 400 MHz) ranging from 0.1 to 0.8. In Table 5, column (3) gives the fraction of linearly polarized radiation ($m_{\rm lin}$) at 400 MHz, and the position angle (P.A.) swing across the pulse profile is given in column (4). These are measurements reported in the literature (Gould 1994; Manchester & Taylor 1977; Hamilton et al. 1977). Rotation measures (RMs) of our pulsars are listed in column (5) of Table 5. Adopting the method described in Gupta et al. (1993), we have estimated the apparent flux modulation index ($m_{r,\rm pol}$) for each pulsar. This method takes into account the differential Faraday rotations across the observing band ($B_{\rm obs}$) and across the pulse profile ($\tau_{\rm pulse}$), and estimates the worst-case values of $m_{r,\rm pol}$ (position angle variations across $B_{\rm obs}$ and $\tau_{\rm pulse}$ are treated as approximately linear, and the ionospheric contribution to the RM is assumed to be ~ 1 rad m^{-2}). The values of $m_{r,\rm pol}$ are listed in column (6) of Table 5. The flux modulation indices ($m_{r,\rm riss}$) given in column (8) of Table 4, which are already corrected for the contribution due to noise modulations, are further corrected for the contribution due to $m_{r,\rm pol}$, and the new values of $m_{r,\rm riss}$ are given in column (7) of Table 5. For 10 pulsars, $m_{r,\rm pol} \lesssim 0.05$, and therefore this effect can be ignored. For six pulsars, $m_{r,\rm pol} \sim 0.1$–0.2, but much smaller compared to their observed flux modulation indices, and hence the effect is only marginal. For PSR B1237+25 and PSR B1929+10, for which a substantial fraction of radiation is linearly polarized (with fractional linear polarizations of 0.56 and 0.79, respectively, at 408 MHz), $m_{r,\rm pol}$ is estimated to be very large (~ 0.4–0.5). We also note that for these pulsars, the measured values of m_r are substantially larger than that of the rest, substantiating the effect of Faraday rotation. On applying the correction, we get $m_r \approx 0.42$ for PSR B1929+10, and $m_r \approx 0.55$ for PSR B1237+25.

B3. EFFECT OF THE EARTH'S ORBITAL MOTION ON MODULATIONS OF SCINTILLATION TIMESCALE

The scintillation pattern speed ($V_{\rm iss}$), which determines the scintillation timescale (τ_d), is predominantly due to the pulsar's proper motion. However, in the exceptional cases of pulsars with low proper motions, contributions due to the Earth's orbital motion ($V_{\rm obs}$) around the Sun and the bulk flow of the density irregularities ($V_{\rm irr}$) may also turn out to be significant, which will modify the "intrinsic" fluctuations of the scintillation timescale caused by RISS. In order to identify data for which these effects may be significant, we quantify the effect of Earth's motion as the expected fractional variation in $V_{\rm iss}$, which is computed as the ratio of change in the transverse component of Earth's motion ($\Delta V_{\rm obs\perp}$) over the observing time span ($T_{\rm sp}$) to the scintillation speed ($V_{\rm iss}$) computed from average values of v_d and τ_d. The values of $\Delta V_{\rm obs\perp}$ and $\delta t_{\rm vobs} = \Delta V_{\rm obs\perp}/V_{\rm iss}$ are given in columns (3) and (4) of Table 6. Estimates of $\delta t_{\rm vobs}$ range from 0.01 to 0.24, but for most pulsars it can be ignored in comparison to m_t. The only exceptions are PSR B1540−06 and PSR B1604−00, for which m_t values are comparable to their $\delta t_{\rm vobs}$, and therefore modulations of their τ_d measurements are not very reliable. It is not possible to get a similar estimate for the effect due to motion of the medium, but it is known to be significantly lower in comparison to the Earth's motion and the pulsar's proper motion. Bondi et al. (1994), based on their 1 year flux modulation studies of low-frequency variables, argue that $V_{\rm irr} < 10$ km s^{-1}. Therefore we assume $V_{\rm irr} \sim 10$ km s^{-1} and estimate the expected modulation in τ_d due to it as $\delta t_{\rm virr} = V_{\rm irr}/V_{\rm iss}$. Our estimates of $\delta t_{\rm virr}$ are given in column (5) of Table 6, from which one can see that the effect is significant only for PSR B1604−00, for which the values of m_t and $\delta t_{\rm virr}$ are comparable. For PSR B1540−06, PSR B2016+28, PSR B2310+42, and PSR B2327−20, although $V_{\rm iss} < 100$ km s^{-1}, $\delta t_{\rm virr}$ are considerably lower than the measurements of m_t and hence can cause only a marginal increase in the RISS-induced τ_d modulations. Thus modulations of τ_d due to the Earth's orbital motion and/or the motion of the density irregularities are significant only for two pulsars. Nevertheless, neither of the effects is reflected as a large value of m_t for these pulsars.

B4. EFFECT OF INTRINSIC FLUX VARIATIONS ON THE FLUX MODULATION INDEX

It is generally believed that pulsar flux variations seen at timescales of days to weeks are due to RISS. But if there are some intrinsic flux variations occurring over similar timescales, then the measured values of m_r will be overestimates of flux modulations due to RISS. Observations so far, have not conclusively established the occurrence of such intrinsic flux variations. Another possibility is variations over timescales intermediate between our typical durations of observation (2–3 hr) and the interval between the successive measurements (1–2 days). However, we do not find any compelling reason to consider such an effect. Recent studies of flux monitoring suggest that pulsar fluxes are stable over timescales larger than the refractive timescales (e.g., Kaspi & Stinebring 1992). Although the present observations show some evidence for flux variations over timescales longer than our typical time spans of observations (see Paper I for a discussion on long-term stability of flux densities), such effects can be ignored in the present context. While we do not totally rule out any hitherto unrecognized form of intrinsic flux variations, in the absence of any other information we assume that the observed flux modulations are largely due to RISS.

B5. MODULATIONS OF DECORRELATION BANDWIDTH

Unlike the case with the scintillation timescale (τ_d) and the flux density (F), there are no non-ISS effects in our data that can cause modulations of the decorrelation bandwidth (ν_d). Our data are in general free from various kinds of man-made radio noise (mainly due to the geographical location of the ORT). The fraction of data corrupted by different kinds of radio frequency interference (RFI) seldom exceeds a few percent, and are excluded from the analysis. Sample data presented in Figures 1*a*–1*h* and 3*a*–3*m* of Paper I give some idea about typical quality of our data.

The modulations of ν_d can result from phase gradient and/or curvature effects, whereas only the latter is relevant for τ_d and F. But the theoretical treatments incorporate both effects in predicting the modulation index of ν_d. It is possible to correct the measured ν_d at a given epoch for the refraction due to the gradient effects, as seen from the drifting features in dynamic spectra. This issue is discussed in § 2.2.1. Our analysis shows that modulation indices of corrected ν_d, though somewhat lower than those of measured ν_d, are considerably larger than the Kolmogorov predictions given in Table 1. Further, part of our data are associated with "persistent drifts" or nonzero values of mean refractive angles (this aspect is discussed in § 2.3), which go against the expectations based on simple models. PSR B0834+06 (excluding data from session IV), PSR B1919+21, PSR B1133+16, PSR B1604−00, and PSR B2045−16 belong to this category. It is unclear, however, whether in such cases the measured modulation indices of ν_d signify their true values. But we do not consider this to be a strong enough reason to exclude them from the present discussion.

REFERENCES

Anantharamaiah, K. R., Gothoskar, P., & Cornwell, T. J. 1994, J. Astrophys. Astron., 15, 387
Armstrong, J. W., Coles, W. A., Kojima, M., & Rickett, B. J. 1990, ApJ, 358, 692
Armstrong, J. W., Rickett, B. J., & Spangler, S. R. 1995, ApJ, 443, 209
Backer, D. C., Hama, S., Van Hook, S., & Foster, R. S. 1993, ApJ, 404, 636
Bhat, N. D. R., Gupta, Y., & Rao, A. P. 1997, in Lecture Notes in Physics 506, IAU Colloq. 166, The Local Bubble and Beyond, ed. D. Breitschwerdt, M. J. Freyberg, & J. Trümper (New York: Springer), 211
———. 1998a, ApJ, 500, 262
Bhat, N. D. R., Rao, A. P., & Gupta, Y. 1998b, ApJS, in press (Paper I)
Blandford, R. D., & Narayan, R. 1985, MNRAS, 213, 591
Bondi, M., Padrielli, L., Gregorini, L., Mantovani, F., Shapirovskaya, N., & Spangler, S. R. 1994, A&A, 287, 390
Clegg, A. W., Fey, A. L., & Lazio, T. J. 1998, ApJ, 496, 253
Cognard, I., Bourgois, G., Lestrade, J., Biraud, F., Aubry, D., Darchy, B., & Drouhin, J. 1993, Nature, 366, 320
Coles, W. A., Frehlich, R. G., Rickett, B. J., & Codona, J. L. 1987, ApJ, 315, 666
Cordes, J. M., Pidwerbetsky, A., & Lovelace, R. V. E. 1986, ApJ, 310, 737
Cordes, J. M., Weisberg, J. M., & Boriakoff, V. 1985, ApJ, 288, 221
Cordes, J. M., & Wolszczan, A. 1986, ApJ, 307, L27
Cordes, J. M., Wolszczan, A., Dewey, R. J., Blaskiewicz, M., & Stinebring, D. R. 1990, ApJ, 349, 245
Fiedler, R. L., Dennison, B., Johnston, K. J., & Hewish, A. 1987, Nature, 326, 675
Fiedler, R. L., Dennison, B., Johnston, K. J., Waltman, E. B., & Simon, R. S. 1994, ApJ, 430, 581
Goodman, J. J., Romani, R. W., Blandford, R. D., & Narayan, R. 1987, MNRAS, 229, 73
Gould, D. M. 1994, Ph.D. thesis, Univ. Manchester
Gupta, Y., Rickett, B. J., & Coles, W. A. 1993, ApJ, 403, 183
Gupta, Y., Rickett, B. J., & Lyne, A. G. 1994, MNRAS, 269, 1035
Gwinn, C. R., Cordes, J. M., Bartel, A., Wolszczan, A., & Mutel, R. 1988a, in AIP Conf. Proc. 174, Radiowave Scattering in the Interstellar Medium, ed. J. M. Cordes, B. J. Rickett, & D. C. Backer (New York: AIP), 106
Gwinn, C. R., Moran, J. M., & Reid, M. J. 1988b, in AIP Conf. Proc. 174 - Radiowave Scattering in the Interstellar Medium, ed. J. M. Cordes, B. J. Rickett, & D. C. Backer (New York: AIP), 129
Gwinn, C. R., Taylor, J. H., Weisberg, J. M., & Rawlings, L. A. 1986, AJ, 91, 338
Hamilton, P. A., McCulloch, P. M., Ables, J. G., & Komesaroff, M. M. 1977, MNRAS, 180, 1
Hewish, A. 1980, MNRAS, 192, 799
———. 1992, Philos. Trans. R. Soc. London, A, 341, 167
Hewish, A., Wolszczan, A., & Graham, D. A. 1985, MNRAS, 213, 167
Higdon, J. C. 1984, ApJ, 285, 109
———. 1986, ApJ, 309, 342
Kaspi, V. M., & Stinebring, D. R. 1992, ApJ, 392, 530
Kuz'min, O. A. 1992, in IAU Colloq. 128, The Magnetospheric Structure and Emission Mechanisms of Radio Pulsars, ed. T. H. Hankins, J. M. Rankin, & J. A. Gil (Zielona Gora: Pedagogical Univ. Press), 287
LaBrecque, D. R., Rankin, J. M., & Cordes, J. M. 1994, AJ, 108, 1854
Manchester, R. N., & Taylor, J. H. 1977, Pulsars (San Francisco: Freeman)
Narayan, R. 1992, Philos. Trans. R. Soc. London, A, 341, 151
Phillips, J. A., & Wolszczan, A. 1991, ApJ, 382, L27
Rickett, B. J. 1990, ARA&A, 28, 561
Rickett, B. J., Coles, W. A., & Bourgois, G. 1984, A&A, 134, 390
Rickett, B. J., Lyne, A. G., & Gupta, Y. 1997, MNRAS, 287, 739
Roberts, J. A., & Ables, J. G. 1982, MNRAS, 201, 1119
Romani, R. W., Blandford, R. D., & Cordes, J. M. 1987, Nature, 328, 324
Romani, R. W., Narayan, R., & Blandford, R. D. 1986, MNRAS, 220, 19
Shishov, V. I. 1973, AZh, 50, 941
Sieber, W. 1982, A&A, 113, 311
Simonetti, J. H., Cordes, J. M., & Spangler, S. R. 1984, ApJ, 284, 126
Smith, F. G., & Wright, N. C. 1985, MNRAS, 214, 97
Spangler, S. R., & Cordes, J. M. 1988, ApJ, 332, 346
Stinebring, D. R., & Condon, J. J. 1990, ApJ, 352, 207
Taylor, J. H., & Cordes, J. M. 1993, ApJ, 411, 674
Wilkinson, P. N., Spencer, R. E., & Nelson, R. F. 1988, in IAU Symp. 129, The Impact of VLBI on Astrophysics and Geophysics, ed. M. J. Reid & J. M. Moran (Dordrecht: Kluwer), 305
Wolszczan, A., & Cordes, J. M. 1987, ApJ, 320, L35